

# Pediatric Meningeal Diseases: What Radiologists Need to Know

Dhrumil Deveshkumar Patel <sup>1,\*</sup> , Laura Z. Fenton <sup>2</sup>, Swastika Lamture <sup>3</sup>  and Vinay Kandula <sup>1</sup>

<sup>1</sup> Department of Radiology, Nemours Children's Health, 1600 Rockland Rd., Wilmington, DE 19803, USA

<sup>2</sup> Department of Radiology, Children's Hospital Colorado, 13123 East 16th Ave., Aurora, CO 80045, USA

<sup>3</sup> Department of Radiology, Seth GS Medical & KEM Hospital, Acharya Donde Marg, Parel, Mumbai 400012, India; swastikalamture@gmail.com

\* Correspondence: dhrumilrad@gmail.com

**Abstract:** Evaluating altered mental status and suspected meningeal disorders in children often begins with imaging, typically before a lumbar puncture. The challenge is that meningeal enhancement is a common finding across a range of pathologies, making diagnosis complex. This review proposes a categorization of meningeal diseases based on their predominant imaging characteristics. It includes a detailed description of the clinical and imaging features of various conditions that lead to leptomeningeal or pachymeningeal enhancement in children and adolescents. These conditions encompass infectious meningitis (viral, bacterial, tuberculous, algal, and fungal), autoimmune diseases (such as anti-MOG demyelination, neurosarcoidosis, Guillain-Barré syndrome, idiopathic hypertrophic pachymeningitis, and NMDA-related encephalitis), primary and secondary tumors (including diffuse glioneuronal tumor of childhood, primary CNS rhabdomyosarcoma, primary CNS tumoral metastasis, extracranial tumor metastasis, and lymphoma), tumor-like diseases (Langerhans cell histiocytosis and ALK-positive histiocytosis), vascular causes (such as pial angiomatosis, ANCA-related vasculitis, and Moyamoya disease), and other disorders like spontaneous intracranial hypotension and posterior reversible encephalopathy syndrome. Despite the nonspecific nature of imaging findings associated with meningeal lesions, narrowing down the differential diagnoses is crucial, as each condition requires a tailored and specific treatment approach.

**Keywords:** meningeal enhancement; pediatric; meningitis; drop metastasis; pachymeningeal enhancement



**Citation:** Patel, D.D.; Fenton, L.Z.; Lamture, S.; Kandula, V. Pediatric Meningeal Diseases: What Radiologists Need to Know. *Tomography* **2024**, *10*, 1970–2013. <https://doi.org/10.3390/tomography10120143>

Academic Editor: Ronnie Wirestam

Received: 19 September 2024

Revised: 4 December 2024

Accepted: 5 December 2024

Published: 8 December 2024



**Copyright:** © 2024 by the authors. Licensee MDPI, Basel, Switzerland. This article is an open access article distributed under the terms and conditions of the Creative Commons Attribution (CC BY) license (<https://creativecommons.org/licenses/by/4.0/>).

## 1. Introduction

Meningeal diseases in pediatric patients encompass a diverse array of pathologies, including infectious, inflammatory, neoplastic, and other etiologies [1]. These conditions often manifest radiologically as abnormal post-contrast enhancement, nodules, basal exudates or diffuse thickening of the meninges [2]. The significant overlap in imaging appearances among these various meningeal diseases, despite their distinct clinical courses and prognoses, presents a diagnostic challenge for radiologists. For example, in a study by Bou et al., exploring the causes of leptomeningeal enhancement (LME), anti-MOG antibody associated demyelination (MOGAD) comprised 5% of the cases; which has significantly different clinical course than the commonly encountered infectious meningitis [3]. Consequently, a systematic imaging approach in tandem with clinical and laboratory data is essential in classifying these for accurate interpretation and optimal patient management.

In this review, we propose an imaging-based classification of pediatric meningeal diseases to facilitate differentiation among various pathologies. This classification system aims to provide a structured framework for radiologists to approach meningeal abnormalities in children. Particular emphasis is placed on parenchymal and other associated imaging features, as these characteristics often play a crucial role in distinguishing between different meningeal pathologies. The objectives of this review are threefold: to present a comprehensive radiological classification of pediatric meningeal diseases, to elucidate

the patterns of parenchymal involvement associated with various meningeal pathologies, and to delineate the key radiological and clinical features that aid in differentiating these conditions. It is noteworthy that imaging studies frequently precede lumbar puncture in the emergency department setting, and radiologists are expected to provide a report before cerebrospinal fluid results become available [1,4]. Also, the sensitivity of detecting infectious meningitis in infants, reduces if imaged later in the course of the disease [5]. This underscores the critical importance for radiologists to possess a thorough understanding of the imaging differentials of meningeal diseases, enabling them to provide timely and accurate interpretations that guide clinical decision-making and patient management.

## 2. Imaging Based Classification of Pediatric Meningeal Diseases

Radiologically, meningeal pathologies can be broadly divided according to the predominant structures affected (Table 1 and Figure 1). They can be classified as predominantly involving:

1. Meningeal
2. Parenchymal
3. Variable

**Table 1.** Proposed Classification to differentiate meningeal diseases in children based on imaging features.

	Prominent Meningeal Features	Variable	Prominent Parenchymal Features
Infectious	Viral [Except HSV]	Group B Streptococci	HSV
	Algae (Prototheca)	Tuberculosis	Fungal
Autoimmune	Neurosarcoid		Anti-MOG Demyelination
	Guillain Barre Syndrome		ANCA vasculitis
	Idiopathic Hypertrophic Pachymeningitis		NMDA Encephalitis
Neoplastic	Meningioma	Drop Metastasis (Primary CNS tumors)	
	Glioneuronal tumor		
	Meningeal Rhabdomyosarcoma	Systemic Metastasis	
Vascular		Moya Moya disease	PRES
			Pial Angiomatosis
Other	Intracranial hypotension		
	ALK positive Histiocytosis		LCH

HSV—Herpes Simplex Virus 2; Anti-MOG—Anti-Myelin Oligodendrocyte Glycoprotein; ANCA—Antineutrophil Cytoplasmic antibody; NMDA—N-methyl-D-aspartate; PRES—Posterior Reversible Encephalopathy Syndrome; ALK—Anaplastic Lymphoma Kinase; LCH—Langerhans Cell histiocytosis; CNS—Central Nervous System.

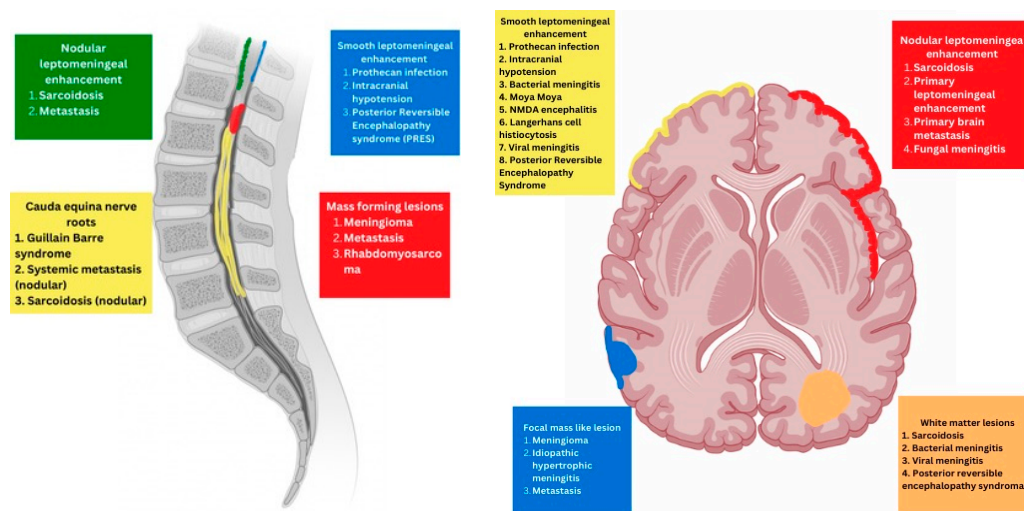


**Figure 1.** Schematic representation of various radiological appearances.

### 3. Predominant Meningeal Features

#### 3.1. *Protothecans*

*Prototheca* species are unicellular algae that are typically known to involve the cutaneous and subcutaneous tissues in humans [6]. Systemic involvement, although rare, can cause meningitis, peritonitis, endocarditis, etc. and is commonly seen in immunodeficient individuals [7]. *Prototheca* spp. infections are usually exogenous and associated with traumatic inoculation from contaminated soil or water. They can also occur from surgery or catheterization, and even insect bites [8]. Exposure leads to chronic granulomatous inflammation with necrosis [6]. Notably, diagnosis of protothecosis may be challenging as it is not easily identified on Hematoxylin and eosin (H&E) or routine fungal stains, and mimics many fungal infections such as *Coccidioides*, *Blastomyces*. Imaging findings include diffuse LME along the cortical sulci and spinal cord, with multiple loculations given the chronic inflammatory response. These loculations characteristically cause mass effect leading to a flattened and deformed spinal cord (Figure 2) [9].

#### 3.2. *Neurosarcoidosis*

Sarcoidosis is a systemic inflammatory disorder characterized by non-caseating granuloma formation [10–12]. Neurosarcoidosis (NS) is uncommon, detected on imaging studies in 15% of the patients, out of which only one-third of them present with clinical symptoms [10,13]. Granulomas, a hallmark of sarcoidosis, can infiltrate cerebral parenchyma, brain vasculature, and cranial nerves [14,15]. Parenchymal involvement leads to motor or sensory deficits, whereas predominant meningeal and subarachnoid involvement leads to cranial nerve deficiencies and vision changes [11]. Contrast-enhanced MRI of the brain and/or the spine is currently considered the standard of care for initial work-up and follow-up in NS [16].

Nodular or diffuse LME, primarily involving the basal meninges, is the most typical finding. It can further spread into the parenchyma via the perivascular spaces [17]. Most cases show focal involvement and are hypointense on T2WI with variable post contrast enhancement [18,19]. Nonenhancing white matter lesions (NEWM), although common, have been shown to have no symptomatic correlation [18]. Optic and facial nerves are frequently involved (Figure 3). The diagnosis of optic neuritis is crucial and regarded as an emergency due to its unfavorable prognosis if not promptly treated [20]. Occasionally [18,21,22], small vessel ischemia related cerebrovascular events occur which manifest clinically with progressive encephalopathy rather than a distinct large vessel stroke [13]. Other rare but important findings include spinal cord and hypophyseal involvement [23]. The mainstay of treatment for CNS sarcoidosis involves corticosteroids to suppress inflammation.



**Figure 2.** Post contrast sagittal T1 brain (A), T1 spine (B), axial T1 brain (C) and spine (D): 17-year-old girl with couple of years of fatigue, shuffling gait, back/lower extremity pain. There is moderate ventriculomegaly (white star). Meningeal enhancement is present around the cervical cord (white arrow). Flattened and deformed brainstem & spinal cord diffusely (curved arrows) and enhancing septae (dashed arrows) within the thecal sac are noted likely from chronic meningitis. Basal cistern enhancement (open arrow) and septae (arrow head) in the lateral ventricles likely reflects sequela of chronic inflammation/infection. Pathology: *Prototheca* Zopfii.

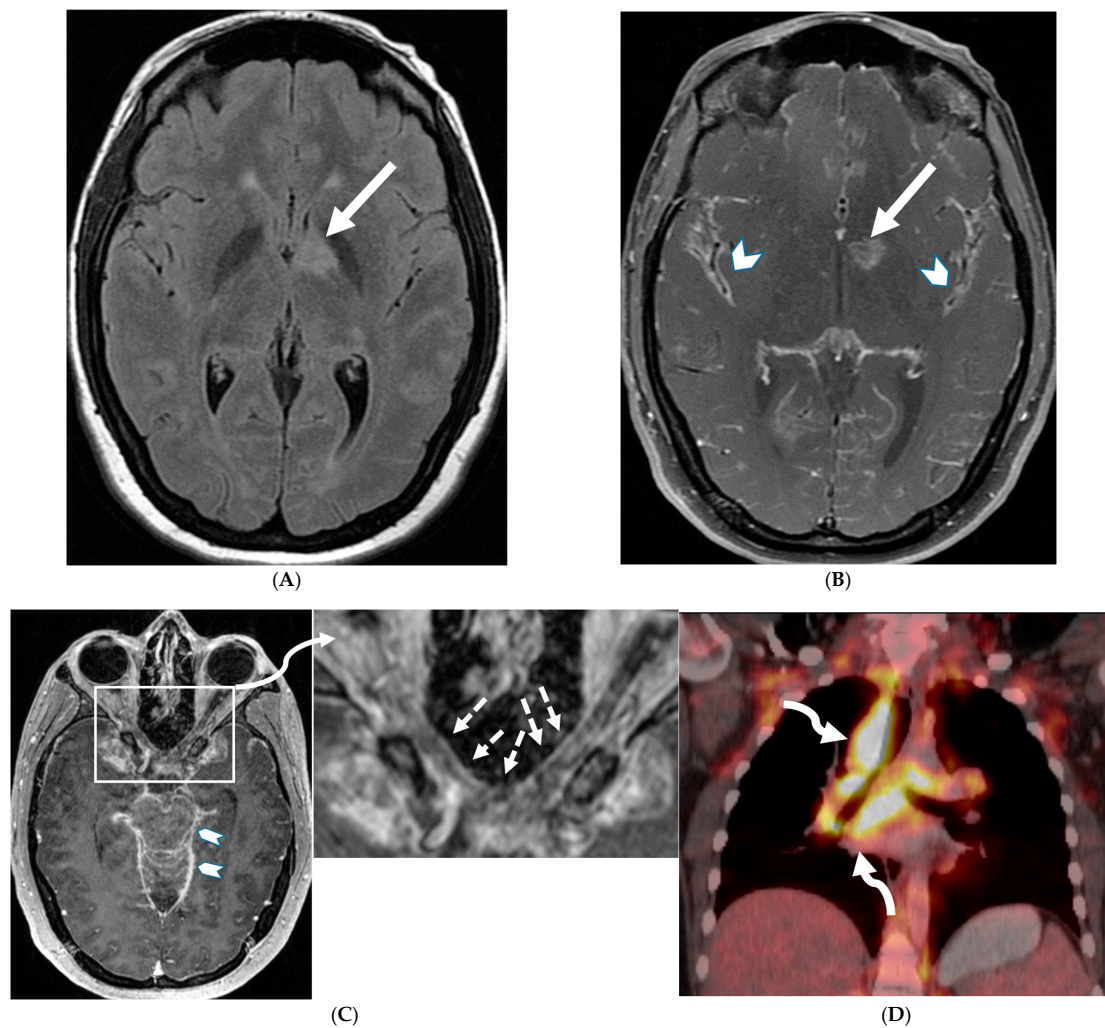


**Figure 3.** 18-year-old presented with headache, persistent vomiting and weight loss. History of sarcoidosis diagnosed 2 years ago. Axial Fluid Attenuated Inversion Recovery (FLAIR) (A), Axial T1 post contrast (B), Axial T1 inversion recovery post contrast (C) and Coronal Positron Emission Tomography (PET) scan (D): There is a heterogeneously enhancing ill-defined area of T2/FLAIR hyperintensity involving the medial aspect of the left globus pallidus (arrows), anterior aspect of the left thalamus and left hypothalamic region. Diffuse enhancement of the basal meninges, tentorium, throughout perisylvian sulci (arrow heads), along the infundibulum, and posteriorly at the craniocervical junction. There is also enhancement along optic nerve sheath (dashed arrows). Features are highly consistent with extensive neurosarcoidosis given the previous history of thoracic sarcoid. PET scan from 2 years earlier demonstrating avid uptake of radiotracer (curved arrows). Radiologically, the differential diagnosis includes tuberculosis and metastatic process. Patient made complete recovery after treatment for sarcoid.

### 3.3. Guillain Barre Syndrome

Guillain-Barré syndrome (GBS) is a rapidly progressive autoimmune disorder affecting the peripheral nervous system usually in response to a prior respiratory or gastrointestinal infection [24–28]. The hallmark presentation of GBS is progressive ascending weakness typically beginning in the legs and spreading to the arms. Areflexia, autonomic dysfunction, and respiratory failure can also occur [29]. Diagnosis is primarily based on clinical presentation, supported by cerebrospinal fluid (CSF) analysis and electrophysiological studies [30,31]. Magnetic resonance Imaging (MRI) is indicated in equivocal cases where excluding other diagnosis is critical and would alter management.

The most characteristic MRI findings in GBS are smooth contrast enhancement of the spinal nerve roots with variable thickening, particularly in the cauda equina region (Figure 4). Selective or prominent anterior nerve root enhancement favors the diagnosis of GBS [32,33]. A higher incidence of cranial nerve abnormalities, particularly the optic nerve, is seen in children with the GBS variant, Miller Fisher syndrome (MFS) [34,35]. Ultrasound imaging of peripheral nerves offers a promising new tool for early GBS diagnosis by detecting enlarged cervical nerve roots early in the disease course [36,37].



**Figure 4.** Post contrast sagittal T1 (A) and axial T1 (B) of the lumbar spine, post contrast axial T1 of the brain (C,D): 14-year-old girl with numbness/tingling, paresthesia and bilateral lower extremity weakness. Patient also has bilateral facial weakness. There is diffuse mild thickening of the cauda equina nerve fibers with enhancement (arrows). Additionally, exiting nerve roots of the cervical and thoracic region also show enhancement. Enhancement of bilateral facial (dashed arrows) and trigeminal nerves is also visualized (curved arrows). Features are in keeping with Guillain-Barre syndrome (acute inflammatory demyelinating polyneuropathy). With involvement of facial and trigeminal nerves, Miller Fisher variant should be considered.

### 3.4. Idiopathic Hypertrophic Meningitis (IHP)

Hypertrophic pachymeningitis (HP) is a rare disorder characterized by localized or diffuse thickening of the dura mater without an attributable cause [38–40]. Recent studies suggest a possible link between IHP and IgG4-related disease (IgG4-RD) [40–42].

The clinical manifestations of IHP vary depending on the location of the thickened dura and resulting nerve compression. Vertebral canal involvement may cause radiculopathy, limb weakness, and sphincter dysfunction [43]. Anterior cranial fossa involvement may present with retro orbital pain, decreased visual acuity, and eye movement disturbance (due to involvement of cavernous sinus or superior orbital fissure). Posterior fossa involvement may cause dysfunction of cranial nerves VI to XII (most common cranial nerve involved is VIII), and cerebellar ataxia [40].

Cross sectional imaging is marked by a thickened hyperdense dura on non-enhanced Computed Tomography (CT), typically along the tentorium, falx, and prepontine brainstem [44]. MRI typically shows relatively hypointense signal on both T1-weighted and T2-weighted images. Contrast-enhanced T1-weighted MR images characteristically reveal marked homogenous or peripheral dural enhancement [44,45].

While meningioma en plaque and tuberculoma en plaque can also thicken the dura mater, their involvement is typically localized rather than diffuse. Additional parenchymal abnormalities (except brain edema) are absent in IHP [44]. Additionally, these conditions usually cause symptoms from mass effect, and not due to entrapment of nerves and blood vessels [46].

### 3.5. Meningioma

Pediatric meningiomas account for less than 5% of childhood brain tumors, with a higher incidence in the second decade of life [45]. They are associated with neurofibromatosis (NF) types 1 and 2, as well as prior radiation therapy [46]. While it was previously thought that pediatric meningiomas had a higher likelihood of being atypical, this is now a topic of debate [47]. Clinical symptoms are non-specific and vary depending on the tumor's location. Although convexity and parasagittal locations are more common, meningiomas can also be found in atypical locations such as the skull base and ventricles [48]. Meningiomas at the craniocervical junction are typically associated with NF-2 [49].

Several imaging features of pediatric meningiomas are similar to those seen in adults: the majority are of the meningothelial type, displaying a hyperdense core on non-enhanced CT (NECT), isointensity to gray matter on T1- and T2-weighted MRI sequences (Figure 5), and moderate post-contrast enhancement. The detection of one meningioma should prompt a thorough search for additional tumors, as one-third of cases are known to be multiple, indicating potential syndromic or radiation-induced associations [49]. A dural tail is less commonly observed, and its absence does not exclude the presence of a meningioma (Figure 5) [49]. Cystic components are more frequently seen in pediatric meningiomas [49]. Intratumoral calcifications and hyperostosis are present in approximately half of the cases [50]. Imaging differentials to consider include dural LCH or Ewing's sarcoma [51].

### 3.6. Glioneuronal Tumor

Diffuse leptomeningeal glioneuronal tumor (DL-GNT) is a recently classified brain tumor (WHO 2016) previously known by various terms such as disseminated oligodendroglial-like leptomeningeal tumor, dysembryoplastic neuroepithelial tumor-like neoplasm and meningeal gliomatosis [52]. It is also associated with precancerous conditions such as KIAA1549-BRAF gene fusion, 1p deletion or 1p/19q co-deletion and Haberland syndrome [53,54].

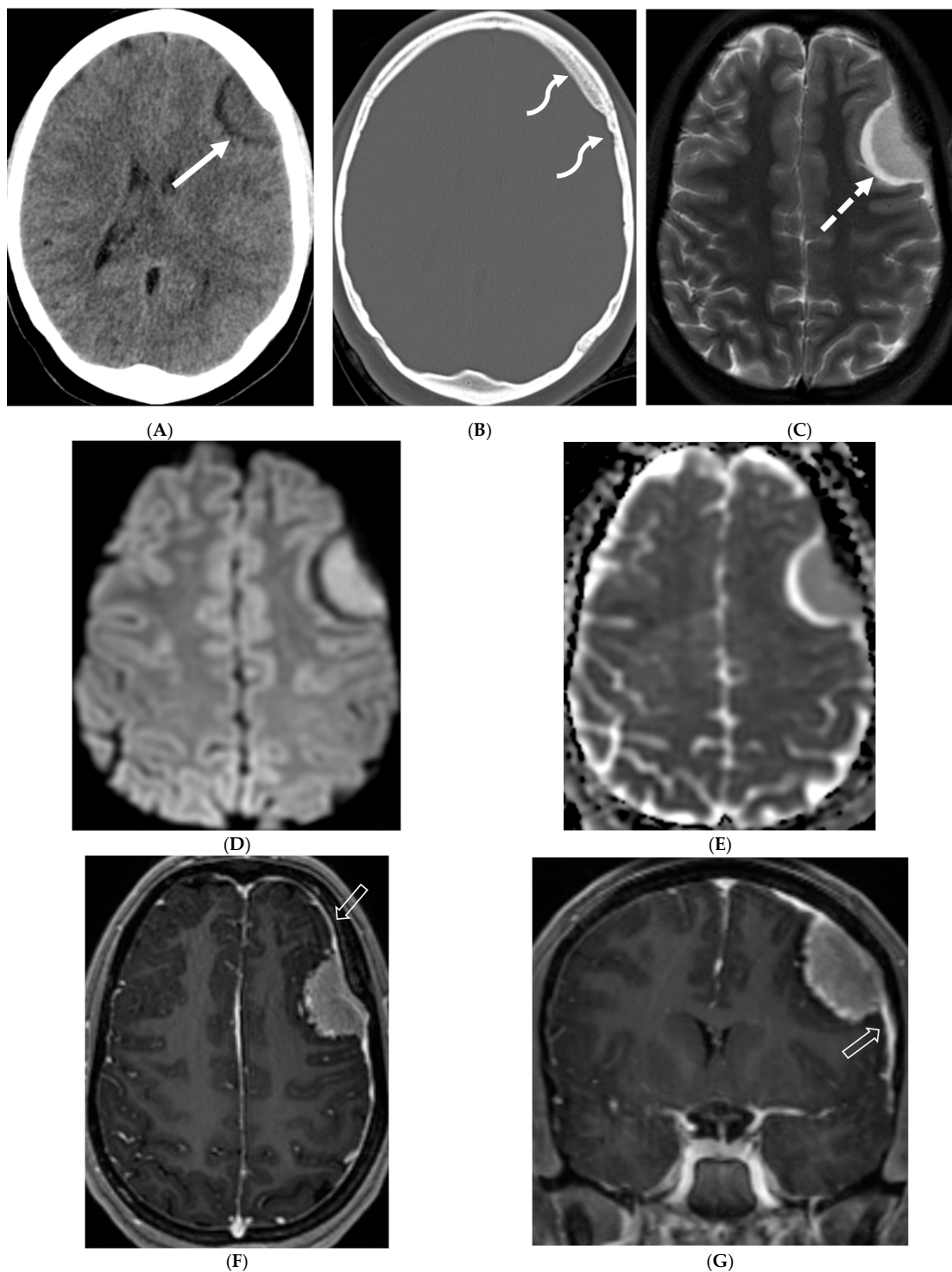


**Figure 5.** Axial CT (A,B), axial T2 fat saturated (FS) (C), Axial Diffusion Weighted Imaging (DWI) & Apparent Diffusion Coefficient (ADC) (D,E), axial and coronal post contrast (F,G): 15-year-old girl with nausea and headaches. CT shows iso-dense dural-based mass in the left anterior cranial fossa (arrow). Adjacent bone is hyperostotic and has irregular cortex (curved arrow). The lesion is isointense with cortex, which is buckled inwards from the mass. A hyperintense rim surrounds the mass representing CSF cleft (dashed arrow). No significant restricted diffusion is noted. The mass enhances intensely and uniformly. A dural tail (open arrow) of benign, nonneoplastic reactive thickening is present adjacent to the left frontal mass, characteristic of classic “typical” WHO grade 1 meningioma.

Although a low-grade neoplasm, leptomeningeal spread is the norm [55]. DL-GNT is characterized by diffuse leptomeningeal thickening, often with basal predominant nodular enhancement [56]. There is invariable involvement of the leptomeninges along the spinal cord in linear fashion [57]. Distinctively, numerous small T2-hyperintense parenchymal cysts are present as a result of fibrosis and obstruction in the subarachnoid space; typically in the inferior frontal and medial temporal lobes [53]. These cysts show incomplete signal suppression on T1 and FLAIR images, possibly reflecting their mucoid nature [53,57]. Engulfment of peripheral nerve roots and invasion of choroid plexus may be seen (Figure 6) [55]. The diagnosis of DL-GNT be pursued with characteristic imaging findings with infectious etiology been ruled out [56].

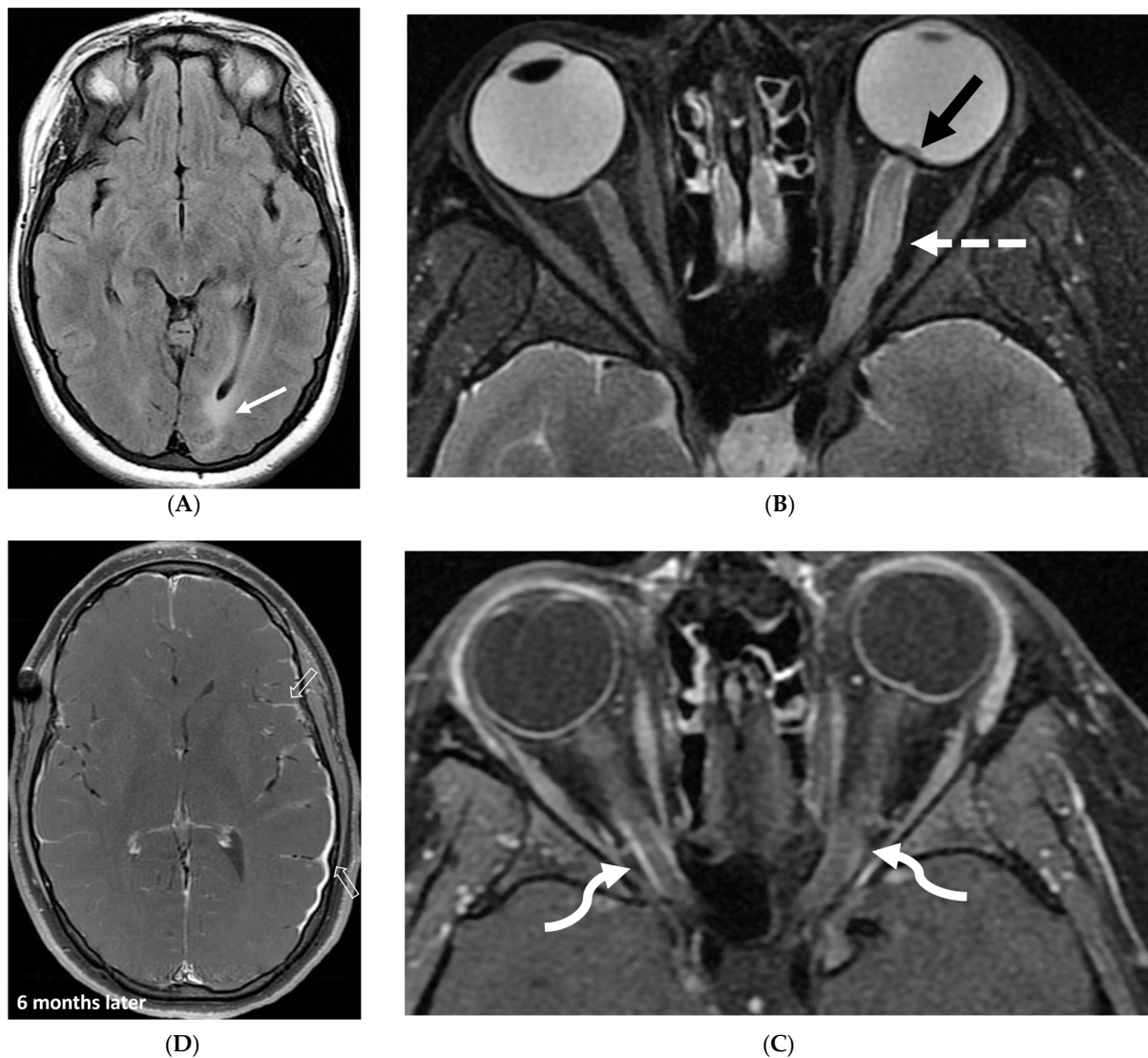


**Figure 6.** Axial FLAIR (A), Axial T2 orbits (B), Axial T1 orbits post contrast (C) and axial T1 post contrast (D): 13-year-old female with headache and blurred vision. Abnormal FLAIR hyperintensity involving the left parieto-occipital periventricular white matter (arrow), and bilateral cerebellar hemispheres. Bilateral papilledema (black arrow) and edematous left optic nerve (dashed arrow). Peripheral optic nerves/optic sheath enhancement in the posterior aspect (curved arrows). Demyelination, infectious and metastatic processes were considered. MRI brain 6 months later with persistent symptoms demonstrates patchy and asymmetric pachymeningeal and leptomeningeal enhancement (open arrows). Pathology: Diffuse Leptomeningeal Glioneuronal Tumor.

### 3.7. Primary Leptomeningeal Rhabdomyosarcoma

Rhabdomyosarcoma, the most common childhood soft tissue sarcoma, is commonly seen in the head and neck, genitourinary tract and extremity [58]. Primary meningeal rhabdomyosarcoma is extremely rare [59,60]. It is hypothesized that the origin of this rare variant is cerebral parenchyma with secondary leptomeningeal spread [61].

Diffuse LME with areas of leptomeningeal thickening and nodularity would be the prominent imaging finding which may cause hydrocephalus. These findings mimic more common entities such as infection (e.g., tuberculosis) or inflammation (e.g., neurosarcoidosis).

Marked focal nodularity and mass effect causing a deformed contour on the spinal cord favor a neoplastic process (Figure 7) [62]. Accurate staging is crucial as the presence of leptomeningeal or multifocal disease have implications on radiotherapy fields and total dose. Additionally, PET-CT scan assists in evaluating for an extracranial primary site [63].



**Figure 7.** 3-year-old boy with 2 weeks history of headache and vomiting. Axial FLAIR (A), post contrast axial T1 FS (B) and sagittal 3D inversion recovery (C) images demonstrate FLAIR hyperintensity in the interpeduncular cistern (curved arrow) and mild hydrocephalus. Extensive meningeal enhancement most prominent at the skull base, basal cisterns, and Sylvian fissures (arrows), but extending throughout the brain. There is meningeal enhancement, with coating of the brainstem extends inferiorly along the cervical spinal cord (dashed arrows). Sagittal T2 (D), sagittal T1 (E) and fat saturated T1 post (F) images show extensive leptomeningeal with predominantly solid and some cystic nodules (curved arrows) on T2 sequence and isointense on T1 (arrows). Lesions predominantly involve the posterior spinal canal, causing mass effect and anterior displacement of the spinal cord. The solid nodules show enhancement after contrast injection and extensive uniform diffuse LME around the cord (dashed arrows). Pathology: Primary Meningeal Rhabdomyosarcoma.

### 3.8. Intracranial Hypotension (IH)

Intracranial hypotension in children is frequently secondary to iatrogenic causes including lumbar punctures, craniospinal surgeries and ventricular shunt drain pressure changes [64]. Spontaneous causes are commonly connective tissue disorders such as Marfans and Ehler Danlos syndromes. Dural tears and meningeal diverticula have been demonstrated in these cases [65]. Beyond headaches, IH can manifest with nausea, vomiting, light sensitivity (photophobia), and stiff neck [66].

MRI features of IH can be explained by the Monroe-Kellie doctrine, which states that the intracerebral volume including blood, CSF and brain parenchyma remain the same. Thus, a decrease in CSF volume promotes dilatation and rounding of the venous sinuses, subdural fluid collections along with dural (pachymeningeal) enhancement which occurs due to vascular engorgement and transudation of fluid into it [67]. Hyperemia of the pituitary gland occurs which may mimic hyperplasia or pituitary tumor. Brainstem slumping or downward displacement of the brainstem, defined as red nuclei below the tentorium and low lying third ventricle below the sella, are highly specific indicators of IH, observed in half the cases. A pontomesencephalic angle of less than 50 degrees and mamillo pontine distance of less than 5.5 mm are sensitive and specific parameters to suggest IH [66].

With regard to spine imaging, in addition to the intracranial features of dural enhancement, venous engorgement and subdural collection, unique findings include meningeal diverticula, dural ectasia and C1–C2 sign (Figures 8 and 9). Additionally, a CT myelogram may identify the precise location of the CSF leak which can be sealed off with a blood patch [65,68].

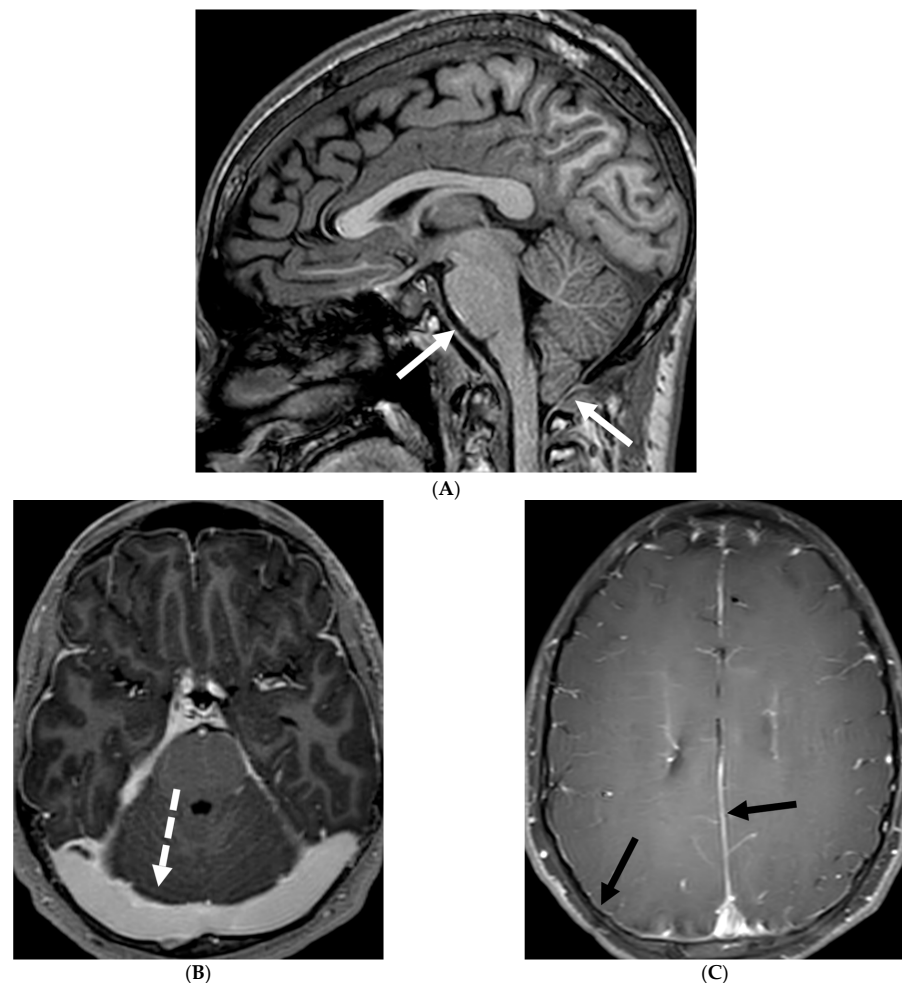
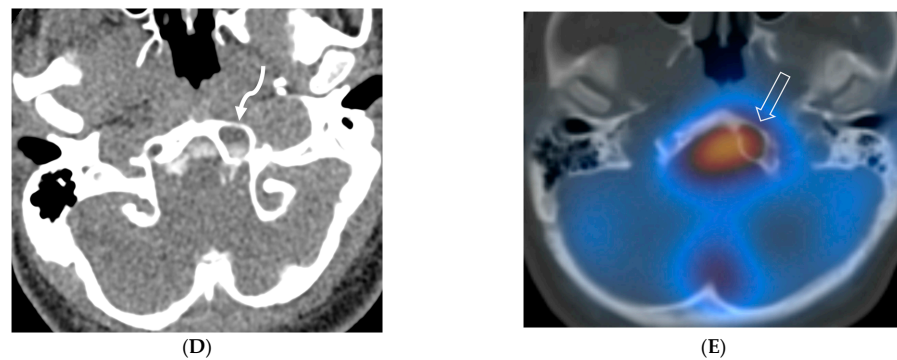


Figure 8. Cont.



**Figure 8.** Sagittal T1 (A), post axial T1 (B,C), axial CT myelogram (D) and technetium 99 m DTPA SPECT-CT (E): 16-year-old with Gorham's disease. There is cerebellar tonsillar herniation and decrease in prepontine cisterns (white arrows). Significant increase in the size of the venous sinuses (dashed arrow). Diffuse pachymeningeal enhancement is seen (black arrows). Cystic-appearing foci at the skull base are in keeping with lymphangiomas with contrast pooling into the lytic lesion (curved arrow). Abnormal radiotracer extravasation in the left clival region correlating with lytic lesion (open arrow). Features are in keeping with intracranial hypotension secondary to CSF leak.



**Figure 9.** Sagittal T2 FS (A), sagittal (B) and axial (C) T1 post contrast: 3-year-old with neck pain post LP. There is diffuse epidural thickening, with increased T2 signal and enhancement, throughout the cervical, thoracic and lumbar spine (white arrows). Several prominent flow voids are seen within the anterior epidural thickening in the upper cervical region (dashed arrow). There is also increased high T2 signal between the occiput and posterior arch of C1, and between the posterior arch of C1 and spinous process of C2 (curved arrows) in keeping with "C1-C2 sign". Findings are related to intracranial hypotension post lumbar puncture.

### 3.9. Alk-Positive Histiocytosis

ALK-positive histiocytosis (APH) is a rare, non-Langerhans cell histiocytosis that can involve the nervous system, including the meninges. While the disease is often seen in infants and young children, it can occur at any age [68]. Neurologic involvement usually presents as seizures, ataxia, headaches, and vomiting [69]. Imaging findings on CT include iso-dense or slightly hyperdense nodules/masses [70]. On MRI, lesions demonstrate isointense or slightly hypointense signals on T1-weighted, isointense or hypointense signals on T2-weighted, with moderate homogeneous focal or smooth ring enhancement [71]. Meningeal enhancement (Figure 10F) can appear segmental and be particularly prominent along the cauda equina [71]. Restricted diffusion is also commonly seen (Figures 10 and 11) [69].

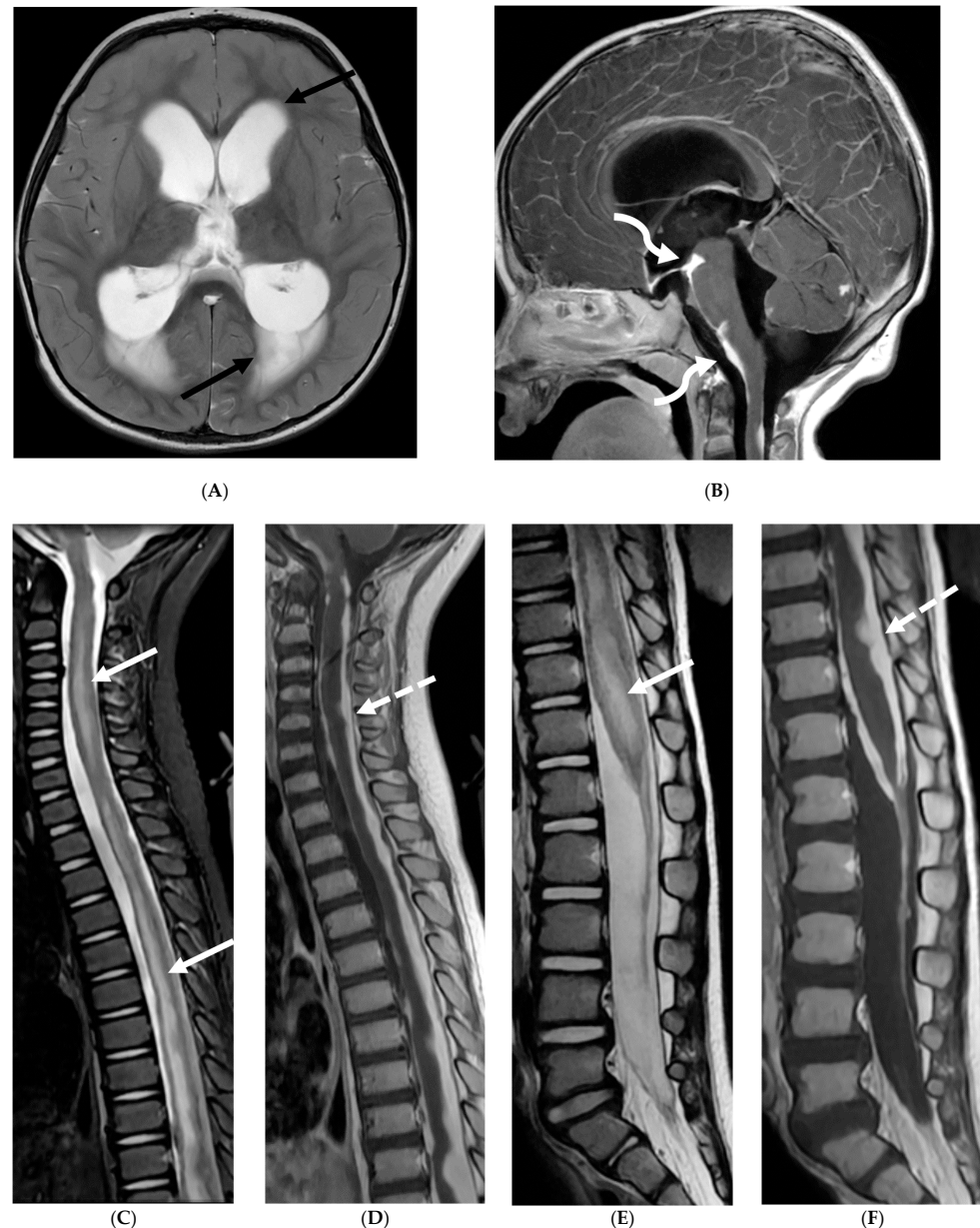
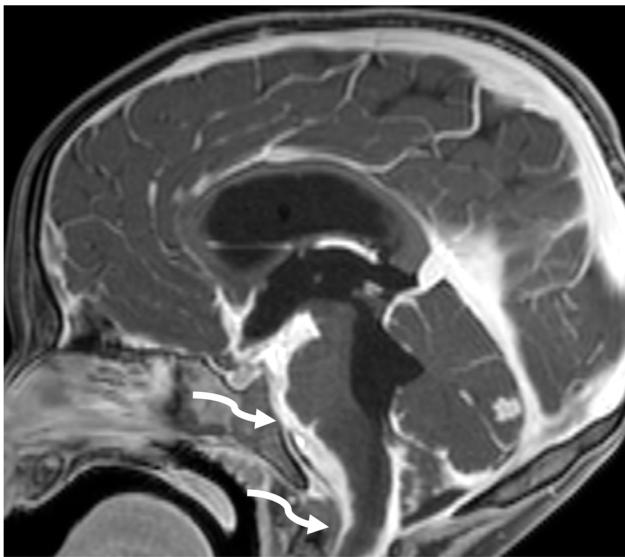
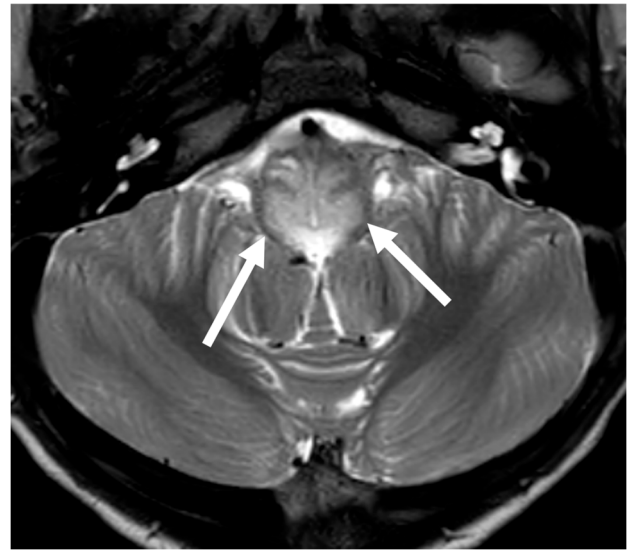


**Figure 10.** Axial T2 (A), sagittal T1 post contrast (B), Sagittal T2 (C,E) and sagittal T1 post contrast (D,F): 20-month-old boy with 2 months of losing developmental milestones and 1 month of emesis, fatigue and dehydration. Ventriculomegaly with transependymal fluid is noted (black arrows). There is posterior fossa leptomeningeal nodular enhancement extending into the upper cervical spine (curved white arrows). Extensive nodular enhancement along spinal cord (dashed white arrows) with cord edema demonstrated in the entire cord (white arrows).

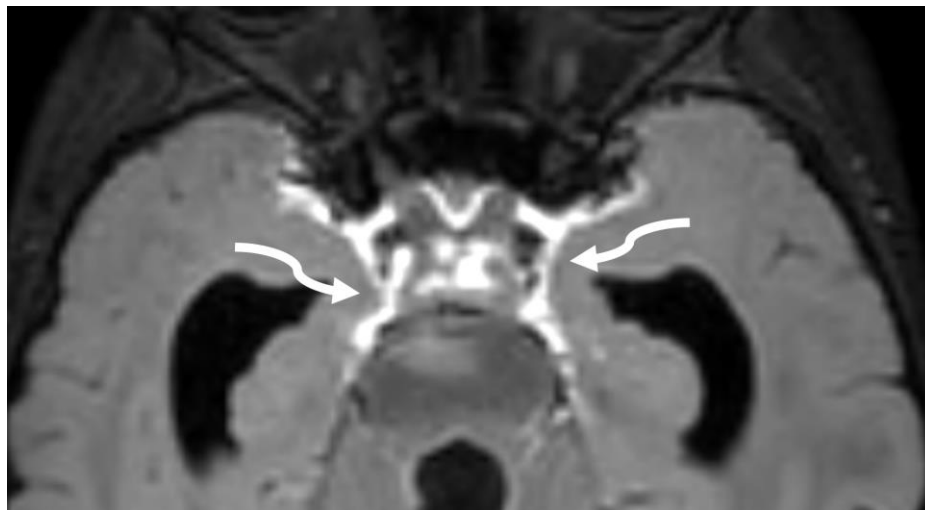
Differentiating APH from other meningeal diseases can be challenging. The most important imaging differential is meningioma. Meningiomas are typically well-circumscribed, dural-based lesions that enhance intensely and homogeneously. Meningiomas often demonstrate a “dural tail”—a thin, linear enhancement extending from the main tumor mass along the dura mater [71]. Another important differential is juvenile xanthogranuloma (JXG), which can also involve the meninges. JXG lesions are typically well-defined, enhancing nodules that are often located near the ventricles or meninges [71]. Ultimately, a definitive diagnosis of APH requires histopathologic and molecular testing, which demonstrates the presence of ALK rearrangement, typically a KIF5B-ALK fusion [72].



(A)



(C)



(B)

Figure 11. Cont.



**Figure 11.** 3 weeks follow up: Post contrast sag T1 (A) and axial FLAIR (B), Axial T2 (C), sagittal T2 (D), Post contrast sagittal T1 (E) and PET/CT (F): Leptomeningeal nodular enhancement along posterior fossa, suprasellar and spinal cord (curved arrows) has significantly increased. There is also new/increased signal abnormality in the brain stem and cord (white arrows). Hypermetabolic spine disease is demonstrated on PET/CT. No osseous involvement is identified on the PET scan. Pathology: Diffuse CNS ALK (Anaplastic Lymphoma Kinase)-Positive Histiocytosis. Bone marrow biopsies, US abdomen and skeletal survey negative for extracranial/extraspinal disseminated disease.

#### 4. Variable Meningeal and Parenchymal Features

##### 4.1. Bacterial Meningitis

Hematogenous dissemination is the primary cause of bacterial spread to the CNS. The most common infective organisms differ according to age with Group B Streptococcus and Escherichia coli commonly affecting neonates and Streptococcus pneumoniae, Neisseria meningitidis, Haemophilus influenzae (decreasing due to vaccination) occurring in infants and children. Post contrast T1 and FLAIR sequences are the primary ones to demonstrate

LME [73]. However, multiple associated parenchymal abnormalities occur in childhood, particularly in neonates due to different causative organisms.

Group B streptococci causes ischemic infarcts along vascular territories in an asymmetric fashion in neonates. Non diffusion restricting extra-axial collections can also occur which tend to resolve on follow up imaging without any sequelae. An important imaging differential in this age group is of hypoxic ischemic encephalopathy (HIE), often with symmetric diffusion restriction in metabolically active regions [74].

*E. coli* is another common neonatal and infantile cause of bacterial meningitis. There is characteristic diffusion restriction in the extra-axial collections along with ventriculomegaly and/or ventriculitis [74]. To note, extra-axial empyema is also common with *S. pneumoniae*, but occur in an older age group. *Serratia marcescens* and *Citrobacter* are two uncommon pathogens causing meningitis in neonates with fulminant disease course. They lead to large parenchymal abscesses with striated appearance on T2W images and foci of susceptibility. *N. meningitidis* causes typical gyriform cortical enhancement consistent with cerebritis predominantly involving the occipital lobes (Figure 12) [74].

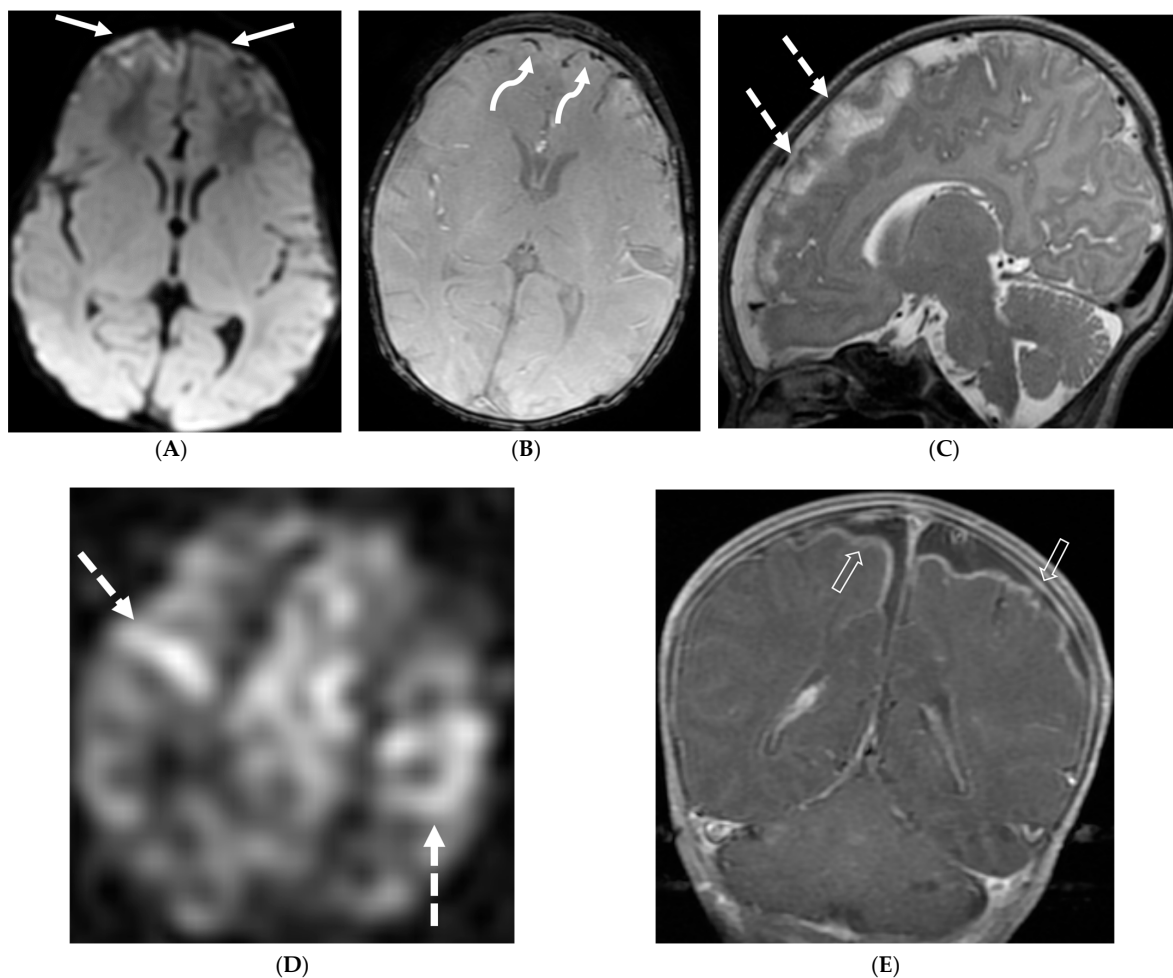


**Figure 12.** Axial DWI (A), axial SWI (B), sagittal T2 (C), axial ASL (D) and coronal T1 post contrast (E): 11-day-old female presented with seizures and lethargic. Restricted diffusion is noted in the sulci along the bilateral frontal convexities, concerning for meningitis (arrows). Curvilinear susceptibility in the extra-axial spaces of bilateral frontal convexities, consistent with thrombosed cortical veins (curved arrows). Cortical T2 hyperintensity is seen in the bilateral frontal and parietal lobes with corresponding hyperperfusion in keeping with extensive cerebritis (dashed arrows). Diffuse leptomeningeal and pachymeningeal enhancement is seen (open arrows). Overall features represent meningitis and cerebritis. Cerebrospinal fluid analysis: Group B streptococcus.

#### 4.2. Tuberculosis

Tuberculous meningitis (TBM) is a severe form of extrapulmonary tuberculosis, associated with high morbidity and mortality rates in those under 5 years old. Case fatality rate reaches up to 20% and only one-third of the patients having no long term neurological sequelae [75]. In developed countries, while the overall incidence of tuberculosis has declined, TBM remains a concern in pediatric populations, particularly among high-risk groups such as immunocompromised children and those from TB-endemic regions. Clinical presentation in children can be subtle and nonspecific, especially in younger age groups. Initial symptoms may include low-grade fever, irritability, poor feeding, and vomiting, which can progress to more severe manifestations such as altered mental status, focal neurological deficits, and seizures.

TBM is characterized by LME, predominantly smooth and localized in the basal cisterns [76]. In severe cases, this can lead to the formation of basal exudates, visible as enhancing fluid in the basal cisterns [77]. The disease is often accompanied by parenchymal abnormalities, most commonly conglomerated ring-enhancing lesions with characteristic T2 hypointensity due to caseous content, although liquefaction may cause the core to become T2 hyperintense [78]. These ring-enhancing lesions can potentially coalesce to form abscesses. TBM may also present with infarcts in the thalami or basal ganglia due to basal vasculitis (Figure 13) [78]. The meningeal involvement typically occurs through hematogenous spread, and the condition is most prevalent in children and young adults presenting with altered mental status [79]. These imaging findings along with lymphocyte predominant CSF and significantly high protein can be diagnosed as tuberculosis since culture can take weeks.

#### 4.3. Primary Brain Tumor Leptomeningeal Metastases (LM)

Common causes of leptomeningeal metastases from a pediatric intracranial primary tumor are medulloblastoma, embryonal tumor, ependymoma, germinoma, pineal tumor and atypical teratoid rhabdoid tumor. The primary theory suggests that tumor cells breach the pia mater and ependyma, gaining access to the cerebrospinal fluid (CSF). These cells then disseminate via the CSF, eventually settling along the spinal meninges [80]. The most common locations are thus, lower-thoracic and lumbar spine, located along the dorsal cord as CSF flow is from brain to the spine dorsally [81].

Currently, contrast-enhanced MRI and CSF cytology are the gold standards for detecting LM [82]. Key imaging findings include enhancing circumscribed nodule/s and/or irregular, thickened enhancement along the dorsal spine [81]. Pitfalls in detection of LM include vascular structures along the cord, seen as short segments of faint and thin enhancement. Veins are typically in midline, are tortuous and most prominently seen in high thoracic and conus medullaris regions (Figure 14). CSF flow artifacts can mimic LM on MRI, especially in the dorsal epidural space with a wide spinal canal. However, their epicenter in the subarachnoid space location can help distinguish them from true lesions [81,83]. MRI with 3D sequences offers superior sensitivity compared to CSF cytology, significantly reducing artifacts [80].

#### 4.4. Systemic Meningeal Metastases (SMM)

Meningeal metastases from an extracranial primary tumor is a diagnosis with a grave prognosis, reducing the survival to less than 3 months if left untreated. Early and accurate diagnosis is essential for improving patient outcomes [84]. Leukemias and neuroblastoma are the most common primary malignancies in the pediatric population [85,86]. Leukemia is the only one which merits prophylactic treatment to avoid SMM.

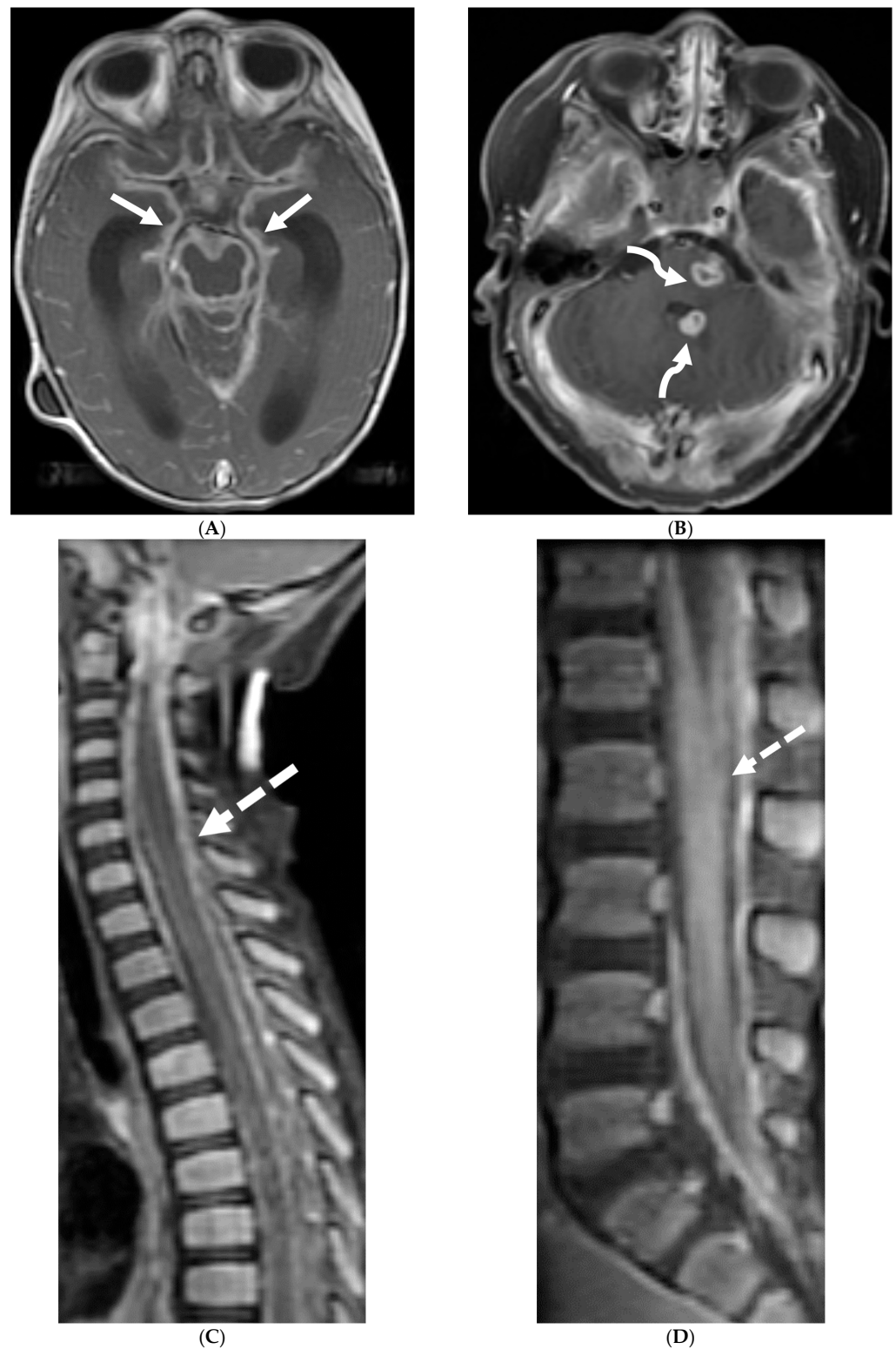


**Figure 13.** Axial T1 FS (A,B) and sagittal T1 fat sat (C,D). 2-year-old girl presented with emesis, fever and status epilepticus. Septic work up revealed tubercular meningitis. Extensive abnormal enhancement is seen in the meninges, prominent in the basilar cisterns (arrows). Ring-enhancing tuberculomas are seen in the cerebellum adjacent to the fourth ventricle and in the brainstem (curved arrows). Diffuse meningeal enhancement and thickening throughout the spinal canal as well as enhancement of the nerve roots is seen (dashed arrows).



**Figure 14.** Post contrast axial T1 (A) and sagittal T1 (B): 3-year-old girl presented with headache, vomiting for 2 weeks and new right sided weakness. Fourth ventricular mass (arrow) with leptomeningeal metastasis (curved arrows). Dural and leptomeningeal metastasis (dashed arrows). Pathology: Anaplastic Medulloblastoma. Axial T1 post contrast (C): 4-year-old girl with headache and vomiting for 2 weeks. There is a partially enhancing mass in the right anterior temporal lobe (arrow) with extensive basal and leptomeningeal metastasis (curved arrow). Pathology: Atypical Teratoid Rhabdoid tumor (ATRT). Axial T1 post contrast (D): 10-year-old boy with vomiting and headaches: There are synchronous tumors in the suprasellar (arrow) and pineal region with hydrocephalus. Subtle LME is seen in the superior vermis (curved arrows). Pathology: Germinoma.

The typical MRI presentation of SMM involves serpentine, nodular, or plaque-like enhancement in sulcal spaces, basal cisterns and along the cauda equina nerve roots [87,88]. Notably, SMM enhancement on post contrast [PC]-T1 images is superior to the PC-FLAIR in contrast to that seen in infectious meningitis [84]. However, in case of a non-enhancing primary tumor, FLAIR and DWI are important sequences to look for SMM. Hydrocephalus and subependymal deposits are other common features found in kids with SMM (Figures 15–17). Positive cytology on CSF analysis, especially with leukemia, is important [89].

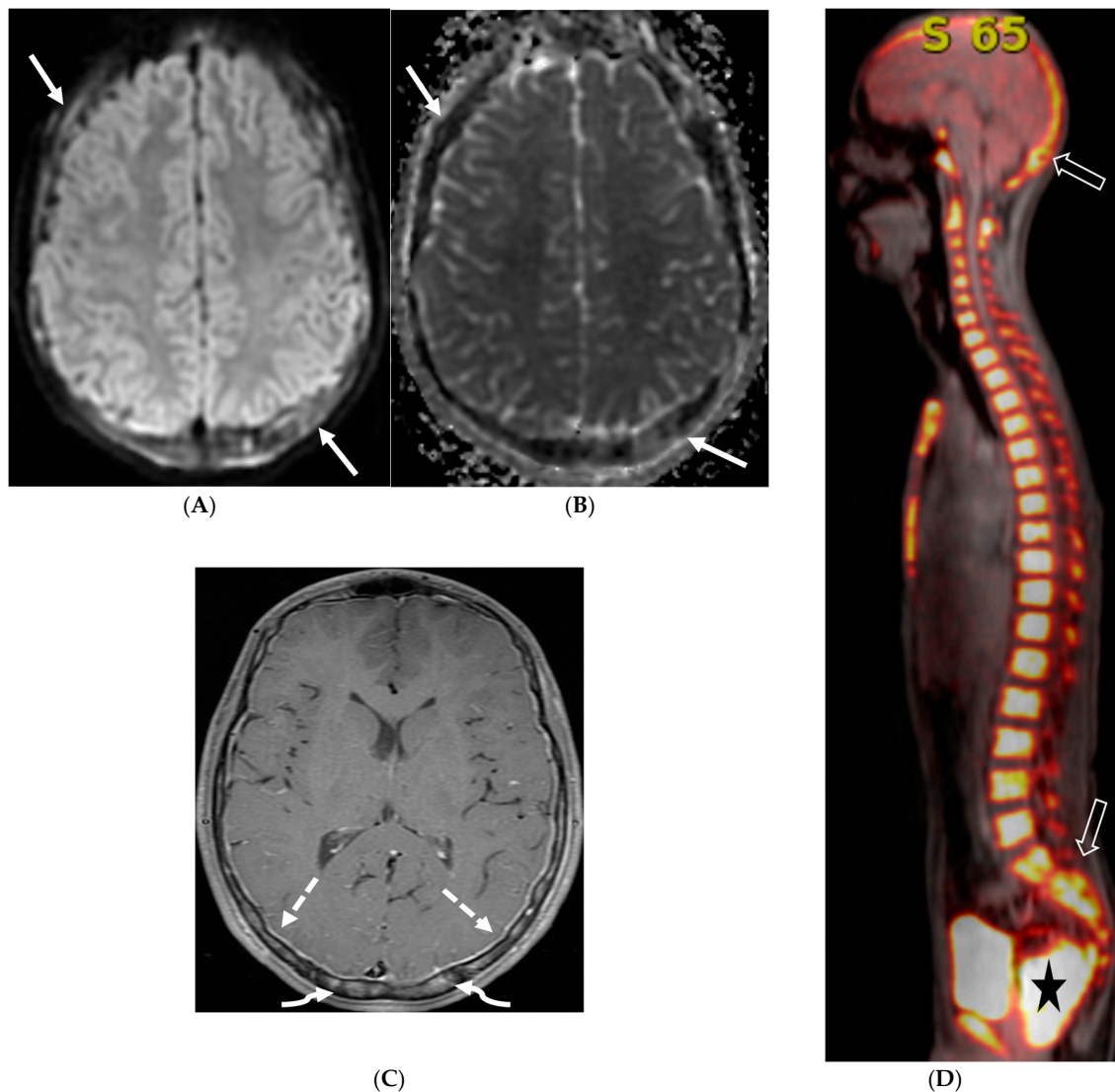


**Figure 15.** Axial DWI (A), axial ADC (B), axial T1 FS post contrast (C) and Fluorodeoxyglucose Positron Emission Tomography (FDG-PET) scan (D): 13-year-old male with bilateral leg pains, headache, fever and weight loss: Blood tests and CT scan were concerning for Burkitt’s lymphoma. There is heterogeneous calvarial bone marrow signal with restricted diffusion (arrows) and patchy enhancement (curved arrows). Diffuse thickening and enhancement of pachymeninges in the supratentorial compartment is noted (dashed arrows). Findings are most consistent with lymphomatous involvement. Multifocal diffuse/heterogeneous pattern of FDG uptake within the axial and appendicular skeleton and the calvarium (open arrows). Intense FDG avid uptake is seen in the presacral mass (star).

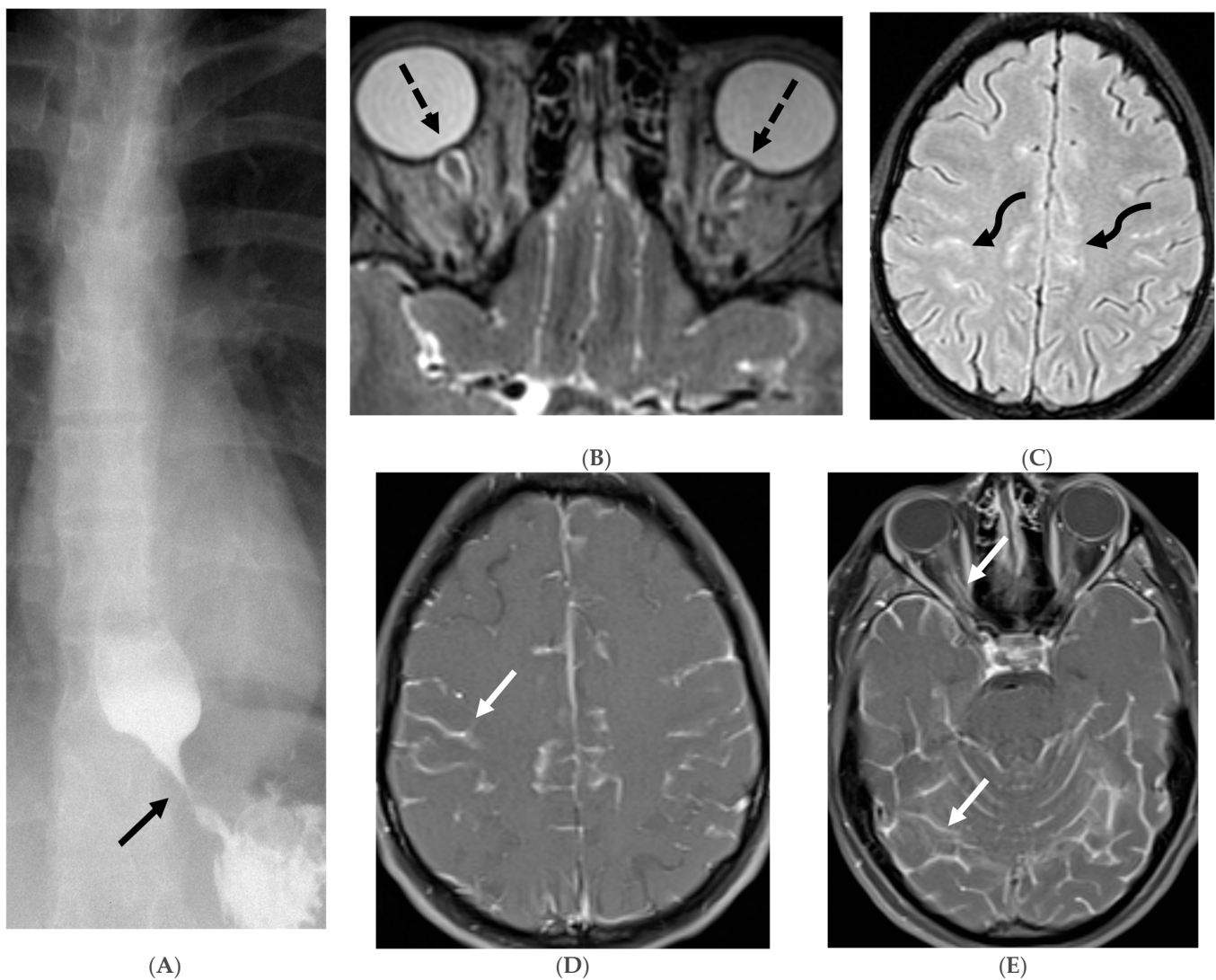


**Figure 16.** 16-year-old female with 4 months history of globus sensation and recent botox injection of lower esophageal junction. Headache and vomiting for past week: Esophagogram (A), Axial T2 orbits (B), axial FLAIR (C) and post contrast T1 (D,E): Narrowing of the Gastroesophageal (GE) junction with beaked configuration and mild distention of the lower esophagus likely from early achalasia (black arrow). There is bilateral papilledema indicating raised ICP (dashed arrows) and sulcal hyperintensity (curved black arrows). Diffuse LME in the supra-and-infratentorial regions and along optic sheaths raising the concern for leptomeningeal carcinomatosis (white arrows). Pathology: Gastric adenocarcinoma metastasis.

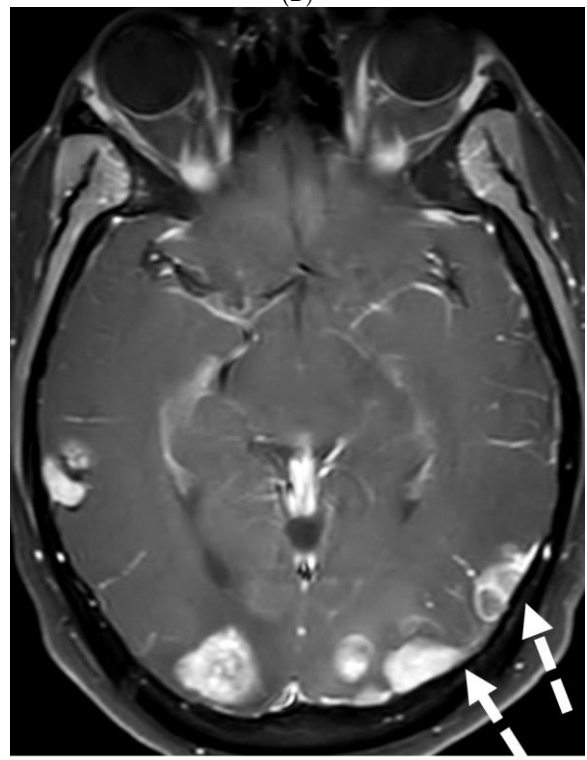
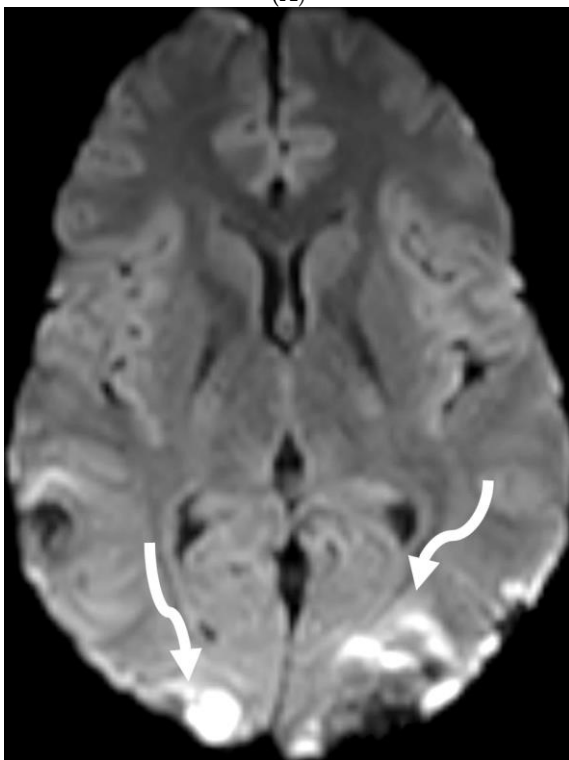
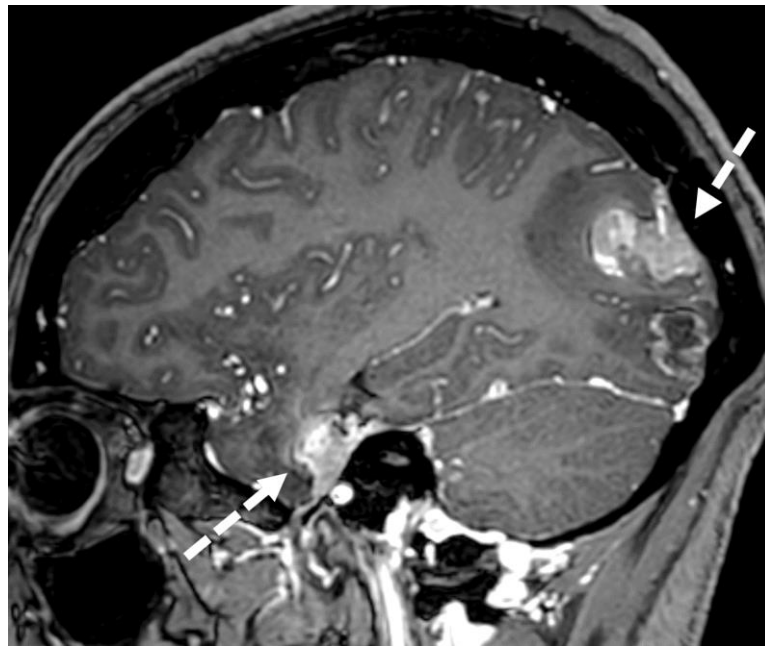


Figure 17. Cont.



(D)

**Figure 17.** Axial T2 FS (A), axial Susceptibility weighted imaging (SWI) (B), axial DWI (C), post contrast sagittal and axial T1 post contrast (D,E): 19-year-old female with history of stage IV neuroblastoma, left paraspinal primary ganglioneuroblastoma, treated with chemotherapy, radiation and bone marrow transplant presents with headache. There are extensive hemorrhagic leptomeningeal masses, both supra and infratentorial region (arrows). The lesions also demonstrate restricted diffusion which could be secondary to internal hemorrhage or high cellularity of the tumor (curved arrows). The larger masses invade the cortex of both cerebral hemispheres, with surrounding vasogenic edema (black arrow). Avid enhancement of the lesions is seen along with overlying dura (dashed arrows). Features are in keeping with extensive leptomeningeal metastatic neuroblastoma.

#### 4.5. Moya Moya

Moya moya disease (MMD) is a complex neurovascular condition characterized by progressive narrowing of the internal carotid terminus and/or the proximal anterior or middle cerebral arteries. Due to chronicity, arterial collateral vessels develop to bypass the narrowing. These collaterals can be basal, leptomeningeal or transdural, arising from perforating arteries, typically coursing through the meninges [90]. These collaterals are often small, weak, and prone to bleed or clot.

MRI, the standard noninvasive imaging modality, shows vascular narrowing on T2-weighted images and collateral vessels [91,92]. FLAIR sequence helps in detecting subtle areas of gliosis or chronic white matter ischemia. While DWI remains the optimal sequence for detecting acute ischemia, SWI helps in detecting acute or chronic microbleeds in addition to prominent deep medullary veins in areas with impaired blood flow (depicted as the “brush sign”). MR angiography defines the disease extent.

In children with moya moya, the LME is termed the “ivy sign” as the appearance resembles creeping ivy (Figure 18) [93]. LME arises due to two key factors in MMD, namely neovascularization and retrograde flow from congested pial vessels [94].

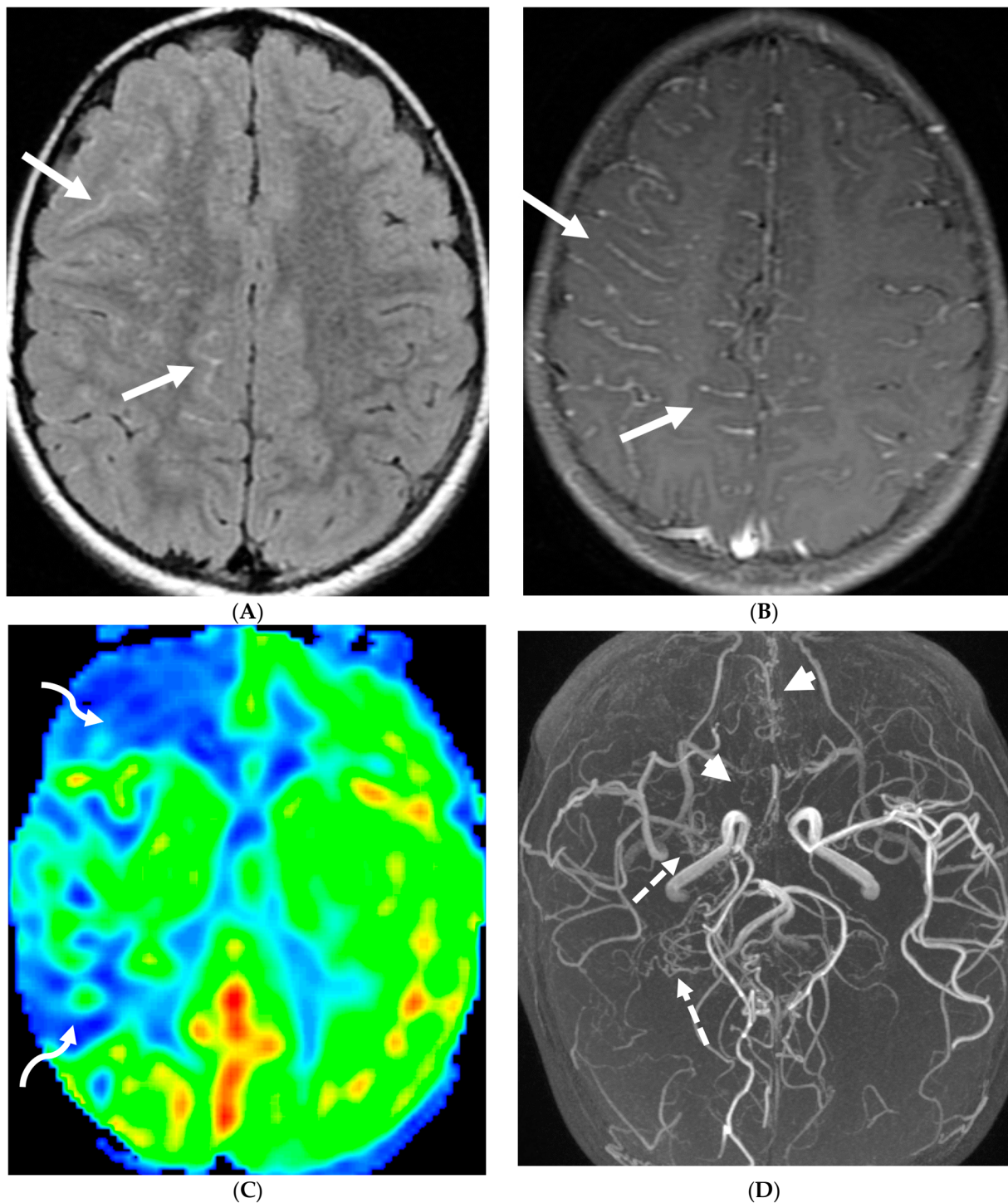


**Figure 18.** Axial FLAIR (A), MRA (B), axial ASL perfusion (C) and axial T1 post contrast (D): 7-year-old girl with Down's syndrome: Abnormal FLAIR hyperintense signal with LME along the right cerebral convexity sulci, predominantly in the frontoparietal region representing "ivy sign" (arrows). Asymmetric decreased perfusion in the right frontal and temporal regions (curved arrows). The M1 segment of right MCA is not visualized with extensive moyamoya vessels (dashed arrows). The M2 and M3 branches of right MCA are asymmetrically attenuated. Bilateral A1 segments are not identified with extensive collateralization and diminutive caliber of A2 and A3 segments (arrow heads).

Although LME is a supportive feature in the diagnosis of moya moya, LME is a marker of collateral vessel status and less LME is a marker of severe clinical symptoms and poor postoperative outcomes [95]. In addition, degree of reduction of LME after surgery has been proposed to be a marker of effective surgery [96].

## 5. Prominent Parenchymal Features

### 5.1. Viral Meningitis

Several viruses, such as enterovirus, herpes simplex virus (HSV)-1&2, mumps, varicella, and arbovirus, can infect children, out of which enterovirus is the most common. These organisms have variable LME, ranging from none to diffuse sulcal LME, best demonstrated on post contrast FLAIR over T1 images [97]. HSV is associated with poor prognosis due to associated parenchymal involvement. HSV-1 commonly causes oral herpes in contrast to HSV-2 which typically causes genital herpes in adults. An active/remote HSV 2 infection in the mother increases the risk of neonatal transmission if delivered vaginally.

HSV 2 typically causes diffuse cortical involvement with diffusion restriction, loss of gray white matter differentiation and basal ganglia involvement in early stages [98]. HSV 1 typically occurs in older children and adolescents and leads to asymmetric temporal lobe involvement with relative sparing of the basal ganglia (Figure 19).

### 5.2. Fungal Meningitis

Fungal infections of the central nervous system (CNS) can be broadly categorized into two forms based on the causative organism's size and pathogenesis. Yeast infections (e.g., *Cryptococcus*, *Candida*) are smaller and disseminate hematogenously, resulting in parenchymal granulomas, abscesses, and diffuse leptomeningitis. Mold infections (e.g., *Aspergillus*, *Mucorales*) are larger fungi that are restricted from entering the meningeal microcirculation, leading to more focal disease manifestations such as cerebritis, abscess formation, vasculitis, infarct, and mycotic aneurysm [99]. *Candida* is the most common fungal organism affecting children, typically in preterm and/or low birth weight neonates [100]. The routes of CNS invasion by fungal pathogens include hematogenous dissemination from a distant source (commonly lung), direct inoculation following trauma or neurosurgical procedures, and local extension from adjacent structures like the paranasal sinuses, orbit, or spine [101].

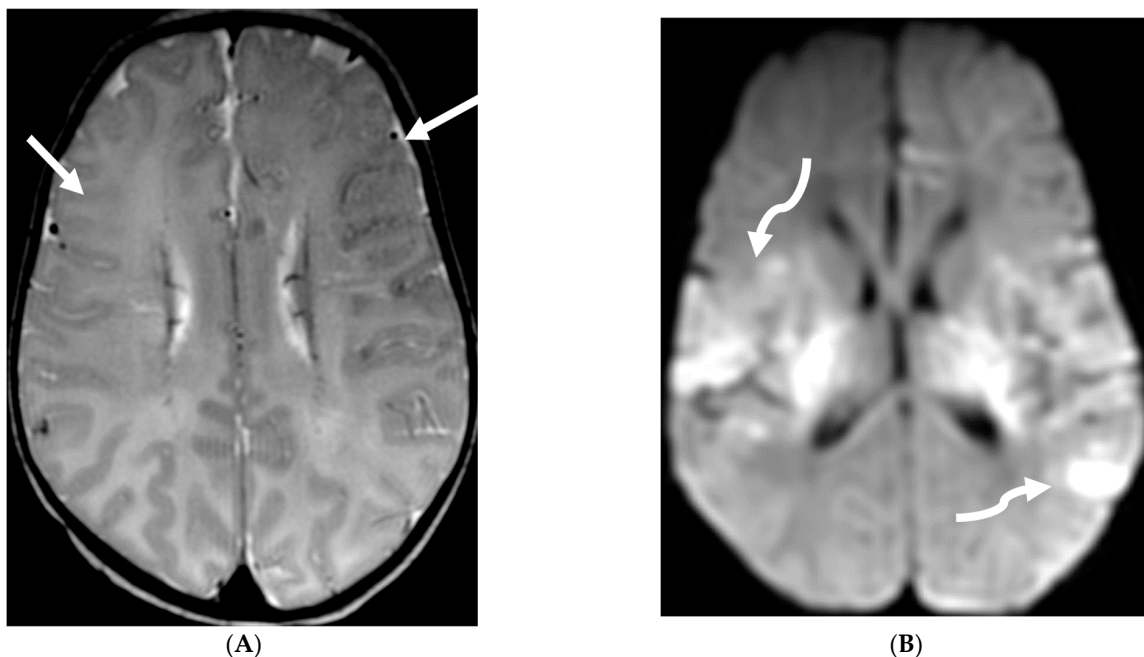
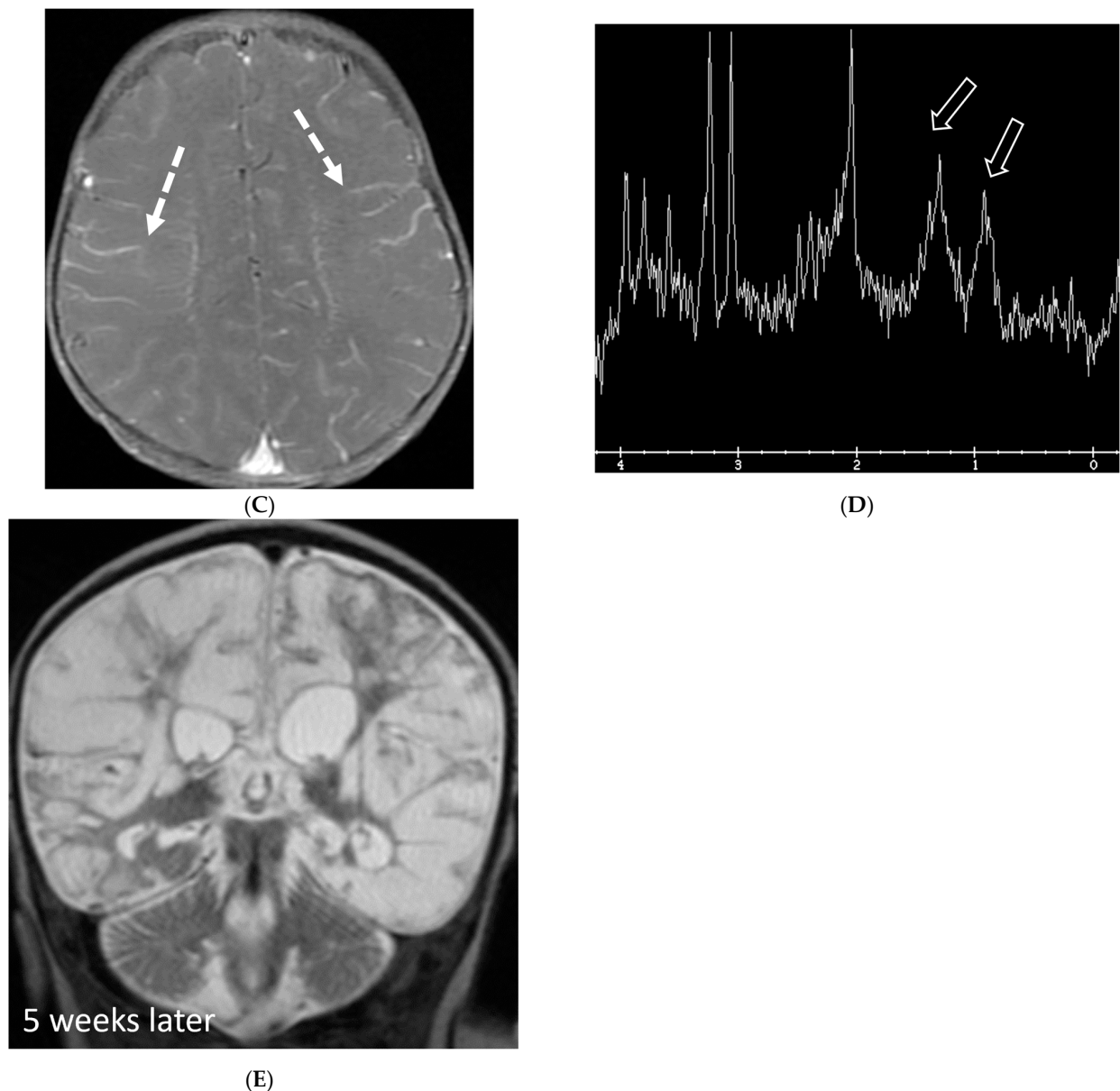


Figure 19. Cont.



**Figure 19.** 17-day-old girl with seizures. Axial T2 (A), axial DWI (B), axial T1 post contrast (C), short TE spectroscopy (D) and coronal T2 (E): There is loss of gray white matter differentiation indicating edema in bilateral frontal lobes (arrows). Extensive ischemic changes involving bilateral frontal, bilateral parietal lobes, bilateral perisylvian regions, bilateral thalami (curved arrows). Extensive LME is identified in the effected regions (dashed arrows). Abnormal elevation of lipid/lactate in both basal ganglia and white matter (open arrows). The above constellation of features are concerning for meningitis/cerebritis. Follow up MRI 5 weeks later demonstrates evolution of extensive ischemic changes into extensive cystic encephalomalacia and gliosis in the supratentorial brain, with ex vacuo enlargement of the ventricular system. CSF analysis: HSV-2.

MRI findings in fungal meningitis include LME, which can be smooth or thick, nodular and irregular, and commonly involve the cortical sulci [102]. While a smooth, linear enhancement pattern is common in viral and bacterial meningitis, it can also be seen in immunocompetent patients with fungal meningitis [102]. Inflammatory exudates containing cell debris, fibrin, and hemorrhage can deposit in the subarachnoid space, leading to arachnoiditis. Protein accumulation in the subarachnoid space shortens T1 relaxation time and results in increased signal intensity on FLAIR sequences [102]. Meningeal adhesions can obstruct arachnoid granulations, leading to impaired cerebrospinal fluid (CSF) drainage

and secondary hydrocephalus. Fungal brain abscesses typically demonstrate a central T1 hypointense and T2 hyperintense core, surrounded by a T1 iso-to-hyperintense and T2 hypointense enhancing peripheral rim (Figure 20) [103,104].

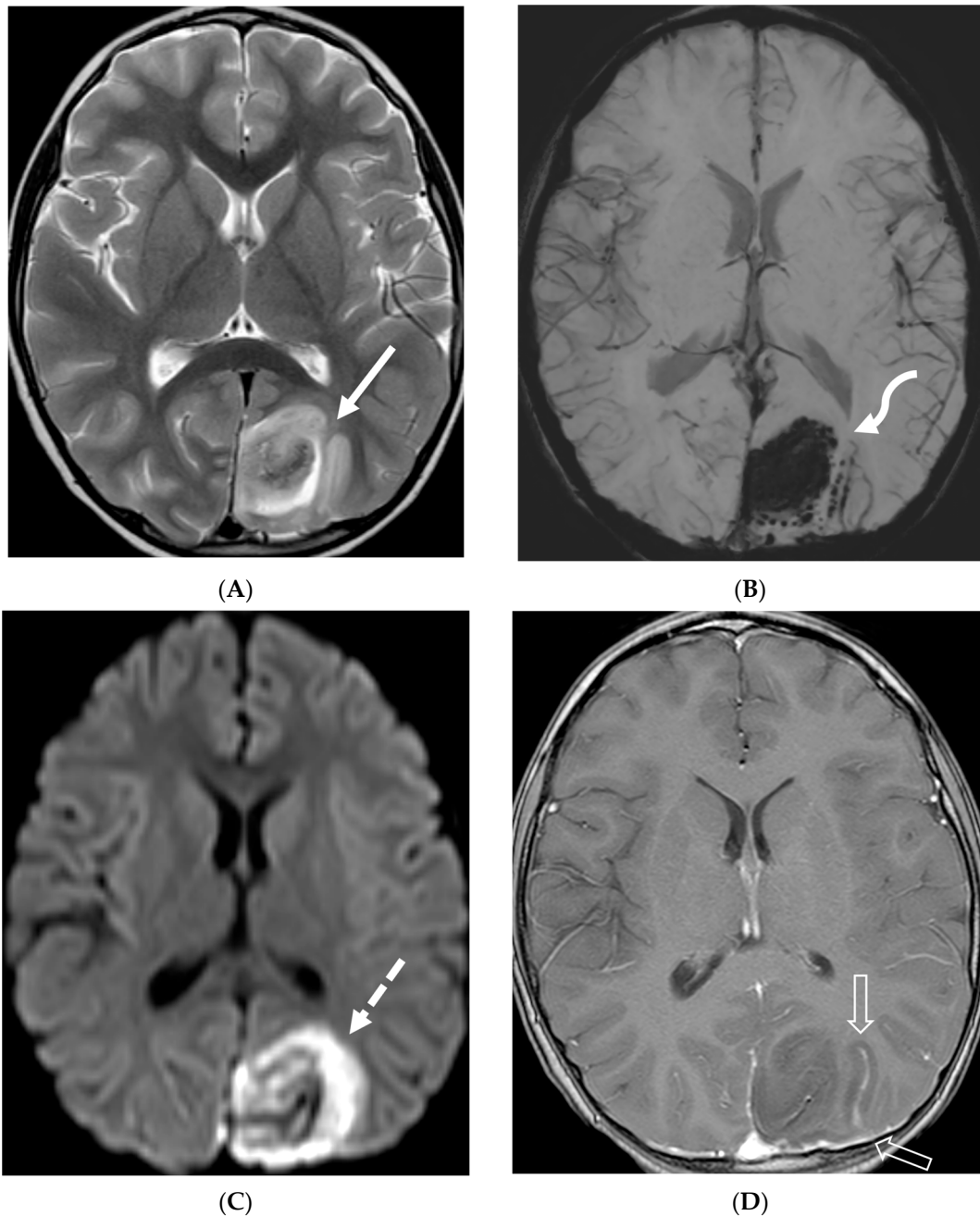


**Figure 20.** Axial T2 (A), axial DWI (B), axial SWI (C) and axial T1 post contrast (D): 4-year-old girl with acute lymphoblastic leukemia, pancytopenia and fever. Treatment started one week before with asparaginase. There is prominently T2 hyperintensity and swelling of the gyri involving the medial aspect of the left parietal occipital cortex (arrow). Multiple small foci of T2 hypointensities are identified within the involved region with corresponding blooming on the susceptibility indicating hemorrhage (curved arrow) and peripheral rim of true restricted diffusion (dashed arrow). Postcontrast images show pachymeningeal and LME in the involved region (open arrows). Features are concerning for fungal infection. Pathology revealed *Rhizomucor pusillis* (thermophilic fungus).

### 5.3. Anti-Myelin Oligodendrocyte Glycoprotein (MOG) Demyelination

Anti-MOG antibody associated demyelination (MOGAD) frequently presents as Acute Disseminated Encephalomyelitis (ADEM) in children and opticospinal involvement in young adults [105]. Bilateral but asymmetric T2 hyperintense lesions occur in thalamus, pons and cerebellar peduncles are common in children [106]. Optic nerve involvement typically presents as a long segment with anterior predominance, in contrast to the posterior predominance seen in Neuromyelitis Optica Spectrum Disorders (NMOSD) and the short segment involvement characteristic of Multiple Sclerosis (MS) [106].

LME has been shown to present early in the disease course and is much more common in children (33%) compared to adults (8%) [107]. Gadde et al. found that 8% of pediatric MOG antibody-associated demyelination cases had only LME without any other central nervous system manifestation. LME when present can be particularly helpful in differentiating from NMOSD [106]. Furthermore, Valencia-Sanchez et al. reported a significant association between LME and cerebral cortical encephalitis in MOG antibody-associated disease. This finding suggests that LME may be an important marker for cortical involvement and potentially more severe disease (Figure 21) [108].

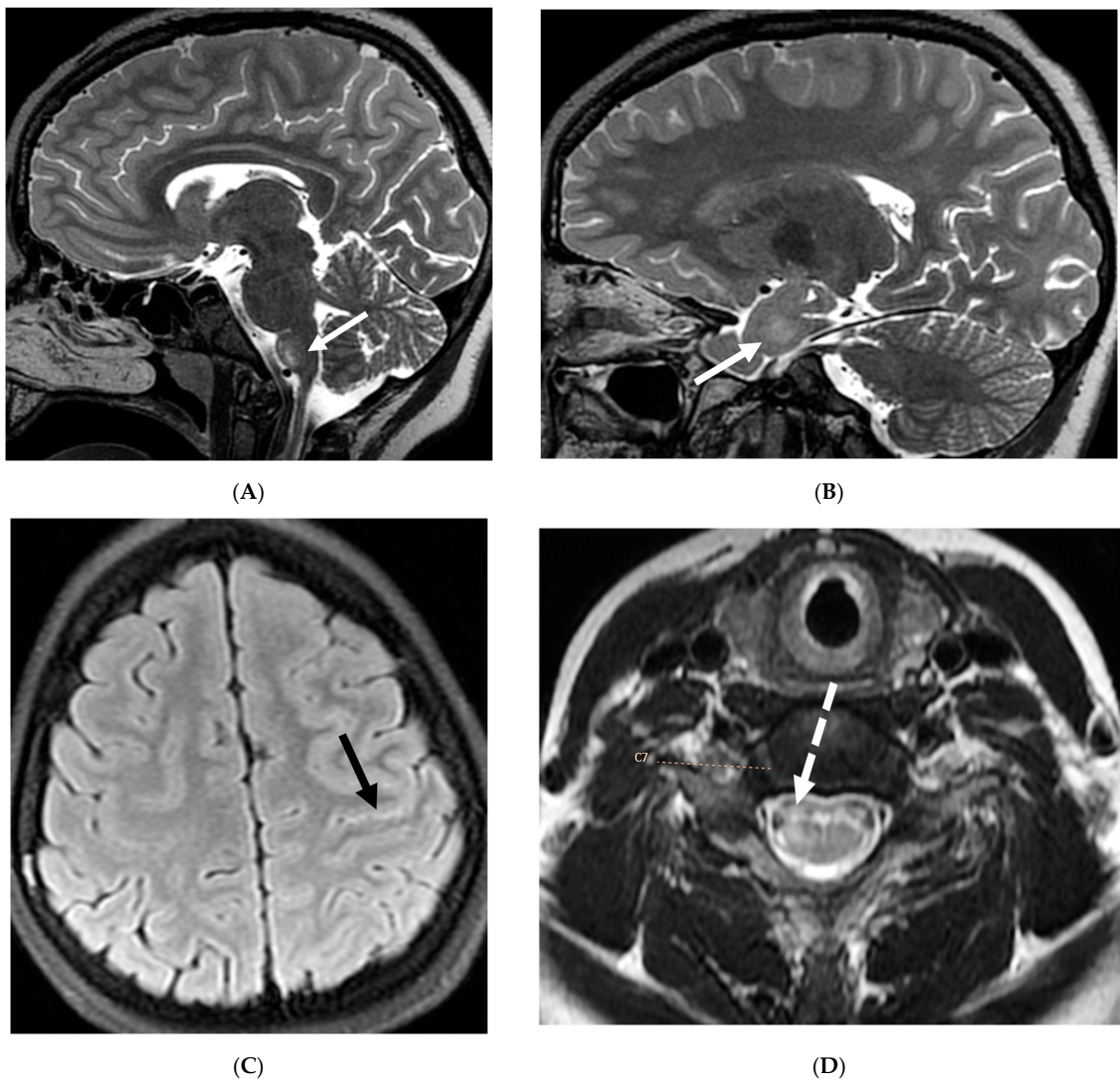
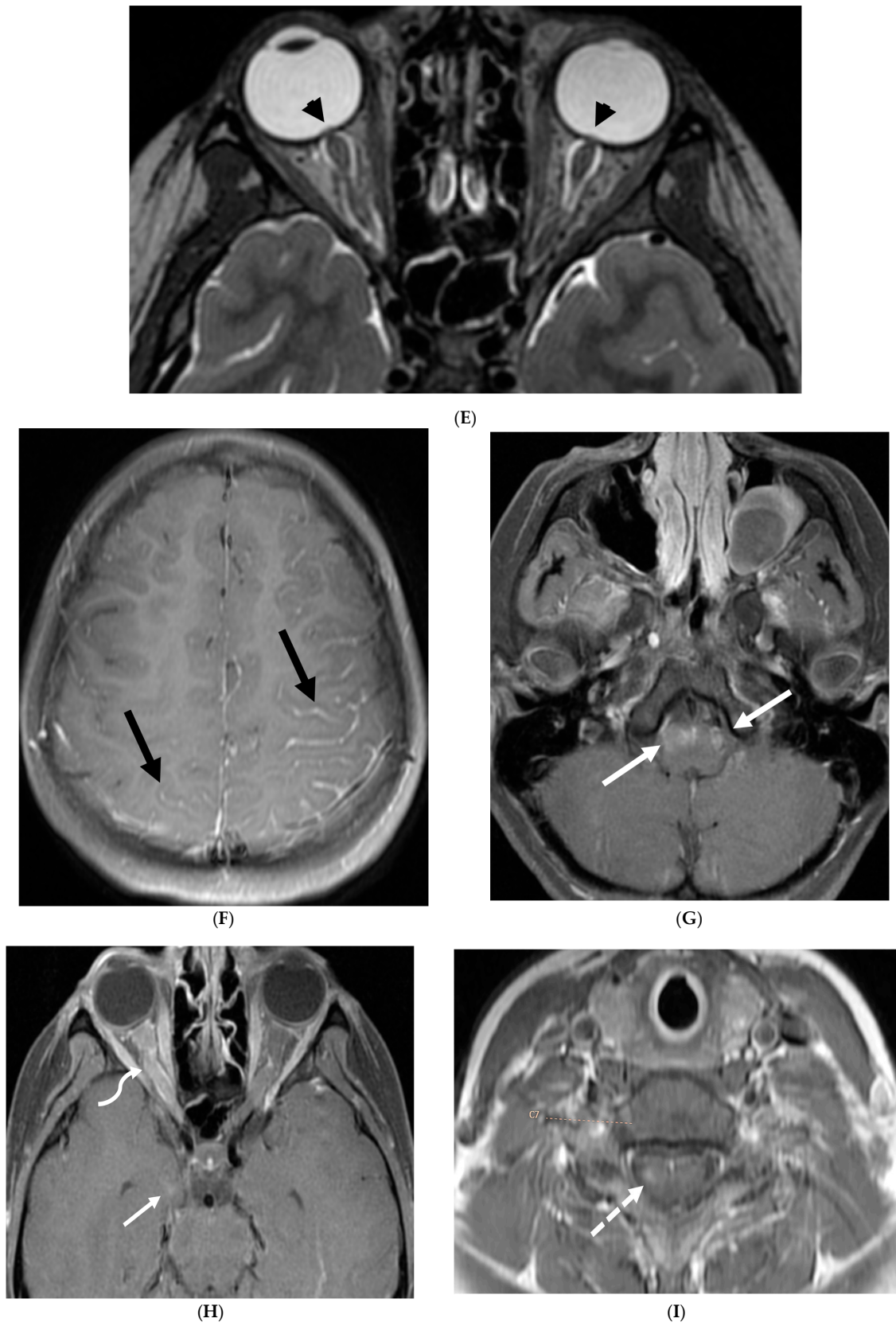


Figure 21. Cont.



**Figure 21.** Sagittal T2 (A,B), axial FLAIR (C), axial T2 cervical spine (D) at the level of C7 vertebral body and Axial T2 orbits (E): 12-year-old girl presented with right focal motor seizure and left temporal lobe slowing on electroencephalogram (EEG). Right eye vision loss and irritability. Ill-

defined areas of signal abnormalities are identified within the RIGHT mesial temporal lobe and bilateral medulla (white arrows). FLAIR hyperintensity is identified on the left central sulcus (black arrow). Small focus of signal abnormality is seen on the right side of the cord at the 7th cervical vertebra (C7) (dashed arrow). There is also bilateral papilledema (arrowheads). Post contrast axial T1 (F,G), axial T1 orbits (H) and axial T1 cervical spine at C7 (I): Asymmetric LME (black arrows) predominantly involving the left cerebral hemisphere, with minimal right parietal involvement is seen. Ill-defined enhancement in the right mesial temporal lobe, and right greater than left medulla (white arrows) corresponds to the signal abnormality. There is right greater than left, optic nerve enhancement (curved arrow). Single small enhancing lesion in the spinal cord on the right at the level of C7 corresponds to the signal abnormality (dashed arrow). Features favor a demyelinating process. MOG antibodies were positive at 1:20 in keeping with Myelin oligodendrocyte glycoprotein (MOG) antibody disease (MOGAD).

#### 5.4. Granulomatosis Polyarteritis (GPA)

GPA is an autoimmune necrotizing granulomatous inflammation associated with anti-neutrophil cytoplasmic antibody (ANCA) vasculitis. This multisystem disorder predominantly affects small vessels, causing endothelial injury and tissue damage in the upper and lower respiratory tract and renal system [109,110]. Neurologic involvement occurs in 20–50% of GPA patients, mediated by three main mechanisms: vasculitis of cerebral vessels, granuloma formation due to contiguous involvement from adjacent paranasal and orbital lesions, and remote granulomatous lesions in brain parenchyma or meninges [111,112]. Patients typically present with headache, altered mental status, and transient ischemic attacks. Pituitary gland involvement can manifest as hyperprolactinemia or diabetes insipidus [111].

Imaging findings in GPA include chronic hypertrophic pachymeningitis (most common) representing granulomatous involvement. This can be diffuse or focal, with the latter showing dural thickening and enhancement adjacent to a sinus or orbit [113]. Tentorium involvement is common, presenting as the 'Eiffel by night' sign [114]. Cerebral vasculitis appears as multiple T2 hyperintense white matter lesions potentially showing diffusion restriction and patchy enhancement. Cerebral atrophy may be observed, attributed to steroid treatment and/or vasculitis. Pituitary involvement can range from normal to enlarged gland size, with thickened stalk and peripheral enhancement. Cranial nerve involvement, particularly of the olfactory and optic nerves, is common due to mass effect from adjacent lesions or hypertrophic pachymeningitis (Figure 22) [112].

#### 5.5. NMDA Encephalitis

Anti-N-methyl-D-aspartate receptor (NMDA) encephalitis is a subtype of limbic encephalitis, the other subtype being paraneoplastic [115]. This autoimmune response to NMDA receptors involved in excitatory neurotransmission results in a constellation of neuropsychiatric and neurological symptoms. It predominantly affects young females and children without an underlying malignancy, although in a subset of cases, particularly in young women, an ovarian teratoma may be associated [116].

The clinical presentation of Anti-NMDA encephalitis often begins with a prodromal phase resembling a viral illness, followed by the evolution of characteristic symptoms over days to weeks. These may include psychiatric manifestations; temporal lobe dysfunction manifesting as memory impairment and seizures; and severe neurological deficits such as autonomic instability and movement disorders (dystonia/dyskinesia) [117,118].

MRI findings in Anti-NMDA encephalitis are frequently nonspecific or absent [119]. However, potential imaging abnormalities may include transient cortical signal enhancement involving the hippocampi, cerebellum, cerebral cortex, insular regions, periventricular white matter, basal ganglia, or brainstem [120]. LME, reflecting meningeal inflammation, may also be observed in conjunction with parenchymal changes (Figure 23) [121]. Notably, the absence of restricted diffusion and hemorrhage on MRI can aid in differentiating Anti-NMDA encephalitis from other etiologies, such as viral encephalitis [120]. It is crucial to recognize that a normal MRI does not exclude the diagnosis of Anti-NMDA encephalitis.

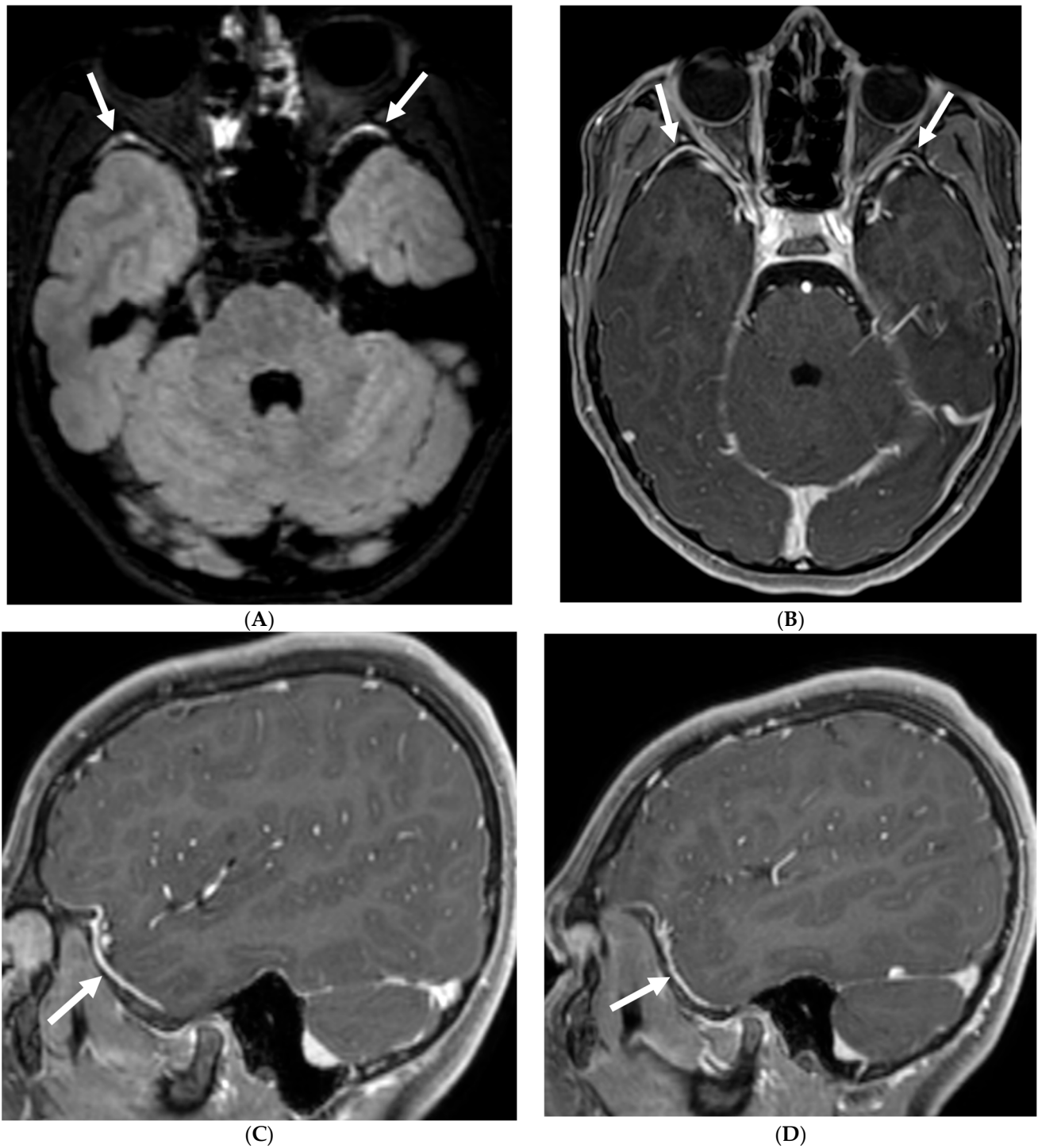


**Figure 22.** Post contrast axial FLAIR (A), axial T1 FS (B), sagittal T1 Right (C) and Left (D): 10-year-old girl with elevated ANCA, headache and mild LUE weakness. There is bilateral anterior temporal smooth dural enhancement (white arrows). Diagnosis: Antineutrophilic cytoplasmic antibody (ANCA) associated vasculitis, likely granulomatosis with polyangiitis.

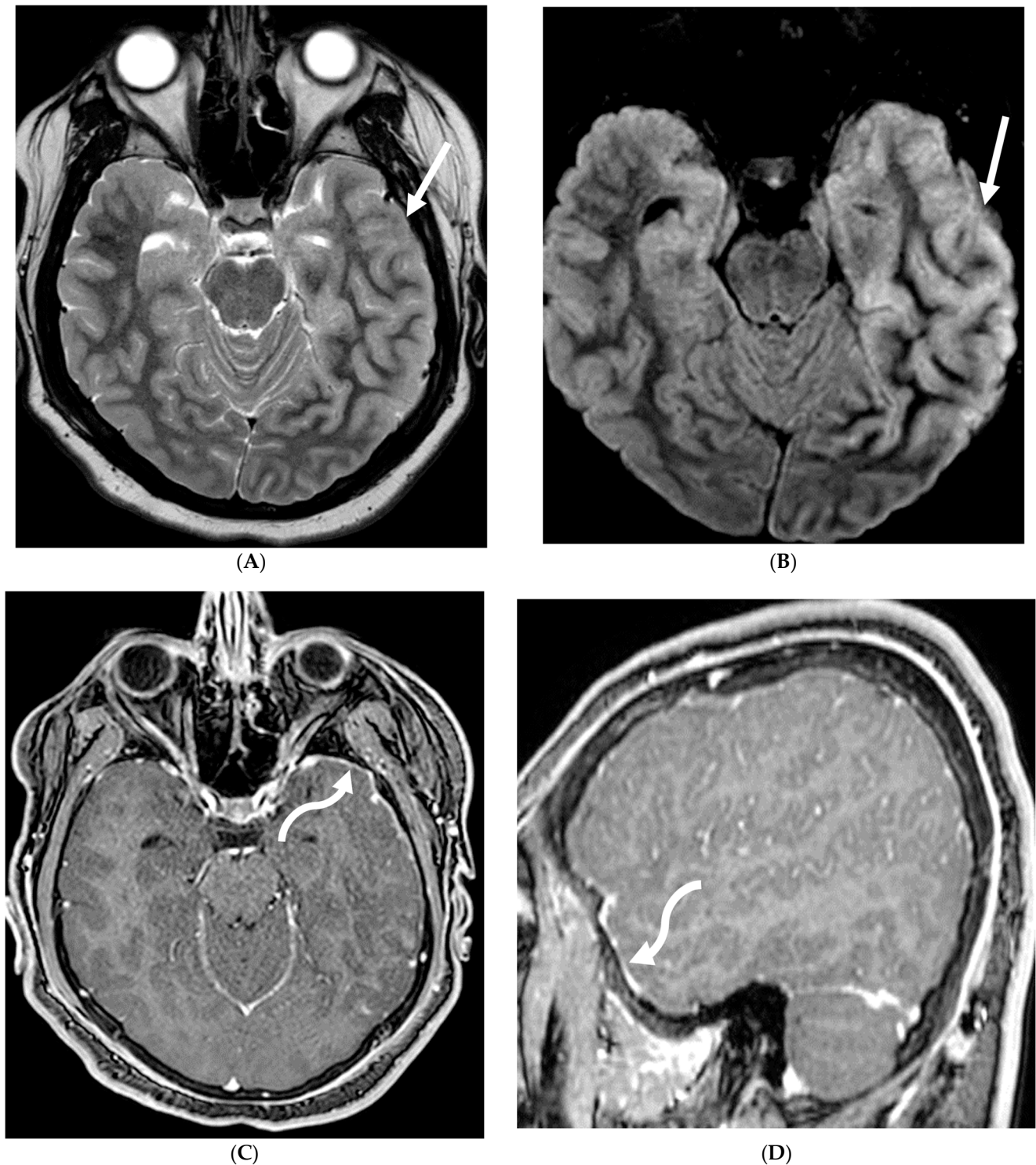


**Figure 23.** Axial T2 (A), post contrast FLAIR (B), axial and sagittal (left) T1 (C,D). 16-year-old male with 3 weeks of headache, photophobia and vomiting. There is asymmetric left cerebral swelling with cortical T2 hyperintensity (white arrows) and anterolateral left temporal LME (curved arrows). Diagnosis: NMDA receptor encephalitis (initially thought to be HSV).

#### 5.6. Posterior Reversible Encephalopathy Syndrome (PRES)

PRES, is a reversible encephalopathy characterized by vasogenic edema, predominantly in the posterior cerebral white matter [122]. The pathophysiology of PRES is likely an autoregulatory dysfunction and/or vasoconstriction of cerebral arteries [123]. Clinical

presentation includes altered consciousness, seizures, headache, and visual disturbance, often developing abruptly and resolving within weeks with appropriate management. The most common predisposing factor is hypertension, particularly with abrupt or intermittent increase in blood pressure [123]. Additionally, nephrotic syndrome, particularly during relapses, is a risk factor due to calcineurin inhibitor use, hypertension, and increased vascular permeability [123].

MRI is the primary imaging modality for detecting PRES [13,16]. T2-weighted and FLAIR images show hyperintense foci in the posterior parietal and occipital lobes, but also frequently involving other regions, including the frontal and inferior temporal lobes and cerebellum [124]. Few tiny to small foci of diffusion restriction may also occur. As per Agarwal et al., leptomeningeal FLAIR signal was seen in about one third of the patients with post contrast enhancement (leptomeningeal +/- cortical) in about 25% of the total population. Majority of these were isolated and had no vasogenic edema [122]. In addition, increased gadolinium dose and delayed imaging increase the incidence of LME (Figure 24) [125].

### 5.7. Pial Angiomatosis

Pial angiomatosis is the hallmark of Sturge-Weber syndrome (SWS), a neurocutaneous disorder characterized by facial port-wine birthmark, ocular abnormality (choroidal angiomas), and leptomeningeal vascular malformation. The pathogenesis involves abnormal persistence and proliferation of embryonic vascular plexuses within the leptomeninges, resulting in tangled angiomatous growths [126]. There is lack of proper venous drainage, leading to rerouting of blood flow through the compensatorily dilated deep medullary veins resulting in venous hypertension and ischemic injury to the underlying cerebral cortex.

MRI with contrast is the preferred modality for evaluation of pial angiomatosis. Early disease stages may show increased cerebral blood flow/volume, characteristic accelerated myelination, LME, and restricted diffusion indicating acute ischemia [127]. LME is thought to be secondary to venous stasis, decreased blood brain barrier or transiently following seizure [128]. Late stage findings include subcortical calcifications, cortical atrophy, prominent deep medullary veins, and ipsilateral choroid plexus enlargement [126].

Characteristic findings on susceptibility-weighted imaging (SWI) are serpentine calcifications along the cerebral gyri [128]. While pial enhancement on postcontrast MRI is the gold standard, some patients with suspected SWS may lack this finding initially, with pial angiomatosis only becoming evident on follow-up imaging (Figure 25).

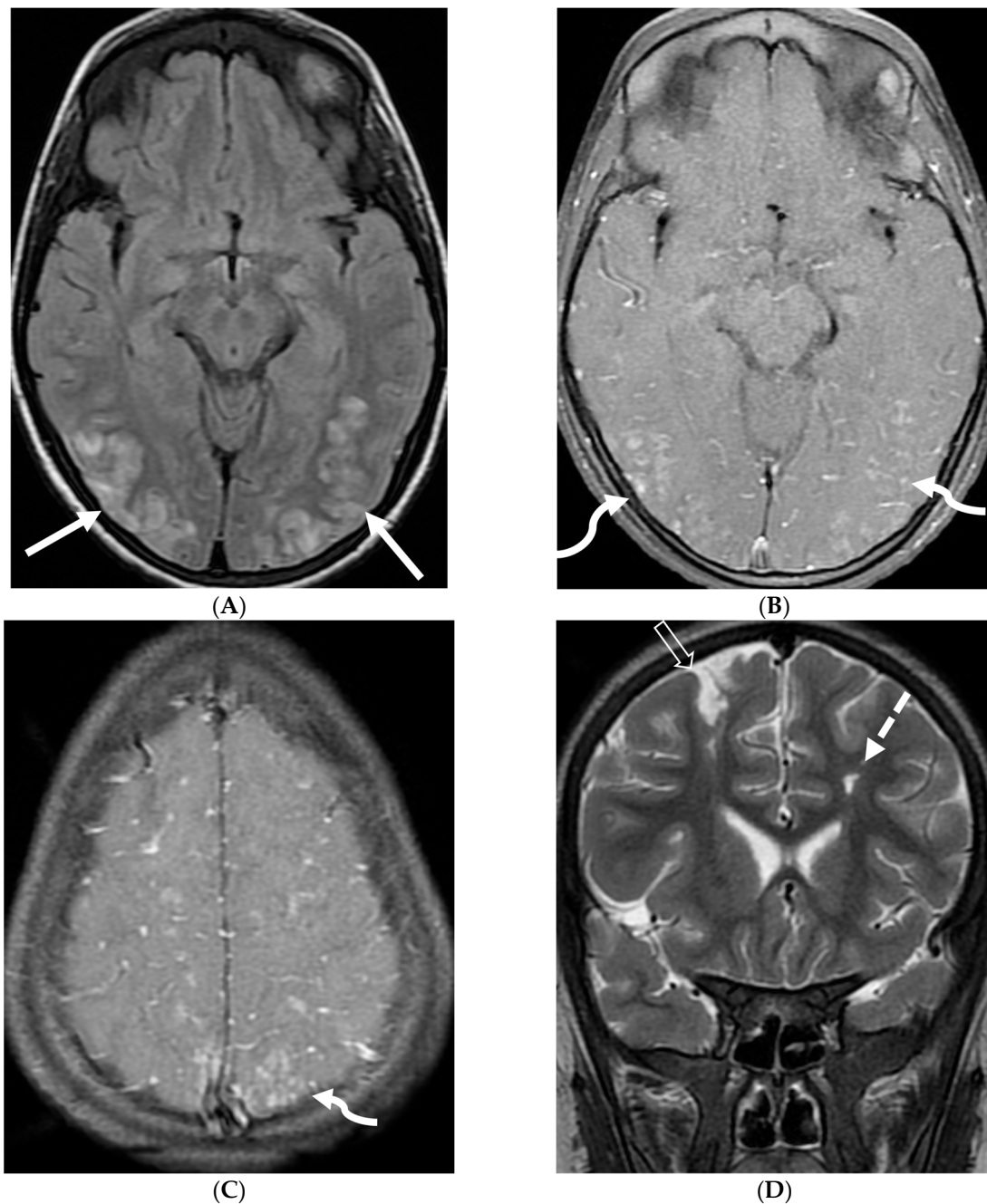


**Figure 24.** Axial FLAIR (A), post contrast axial T1 (B,C) and coronal T2 (D): 6 year 9-month-old male with sickle cell disease presented with altered mental status, seizure and hypertension. Multiple areas of T2/FLAIR signal hyperintensities are seen in a relatively symmetric distribution involving the bilateral occipital, posterior parietal, high frontal and posterior temporal lobes (arrows). Multiple areas of LME are demonstrated in the involved regions (curved arrows). These findings are characteristic of posterior reversible encephalopathy syndrome (PRES). Areas of encephalomalacia and gliosis involving the deep white matter of bilateral frontal lobes (dashed arrow) and a small area of old cortical infarct involving the right frontal lobe (open arrow), secondary to small vessel disease in a patient with sickle cell disease.

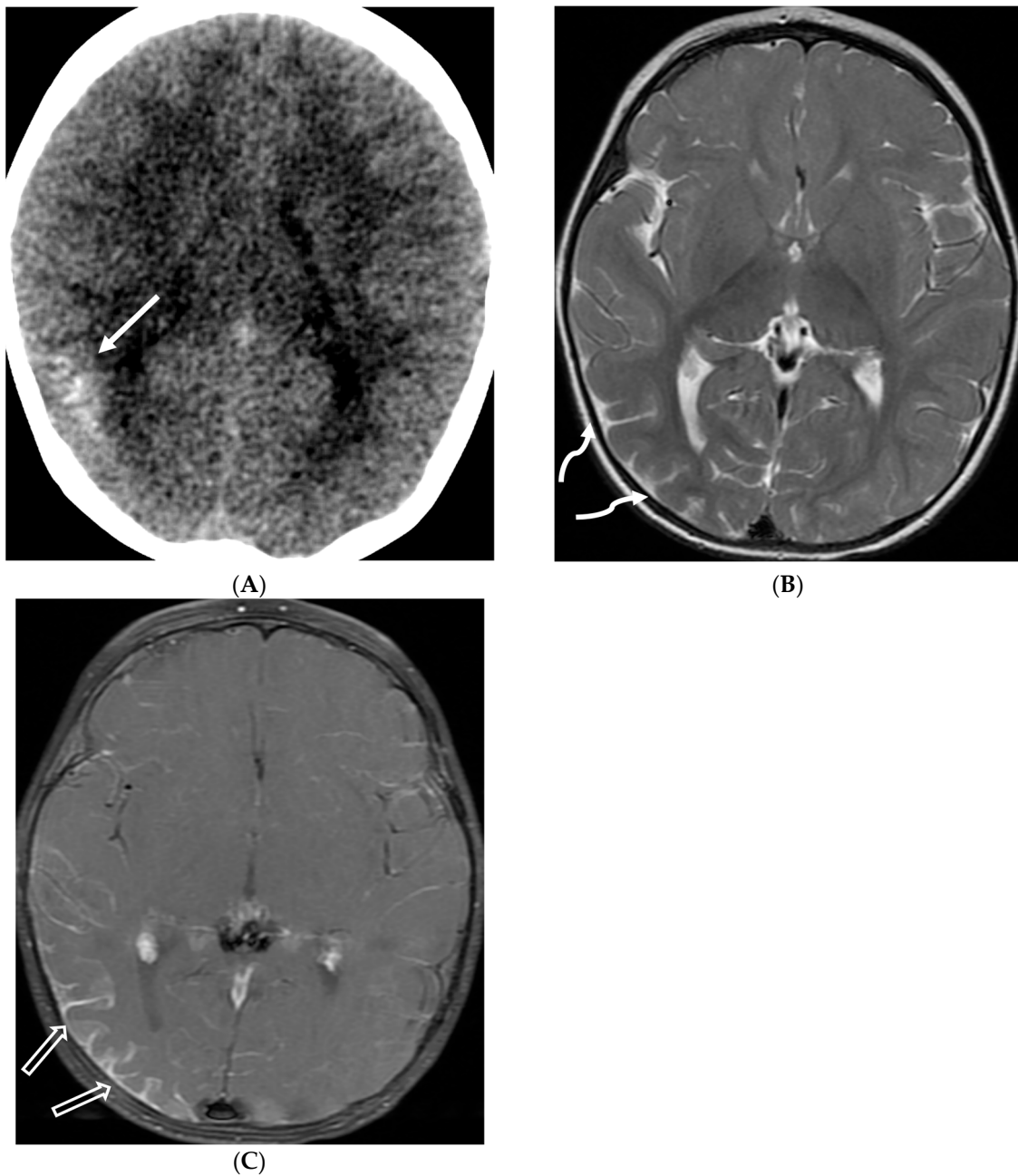


**Figure 25.** Axial CT (A), Axial T2 (B) and Axial T1 post contrast (C): 12-month-old girl presented with focal left sided seizures. There is curvilinear calcification in the right temporal lobe with cortical volume loss (arrow). There is mild parenchymal volume loss and dysmyelination in the right temporal, occipital, and parietal lobes (curved arrows). Thick pial enhancement is seen in the corresponding areas (open arrows). Findings in keeping with pial angiomatosis in the right temporal, occipital, and parietal lobes. Note: Patient does not have port wine stain to support the diagnosis of Sturge-Weber syndrome.

#### 5.8. Langerhans Cell Histiocytosis (LCH)

LCH is an uncommon, often systemic pediatric disorder [129,130]. Clinical course can vary from spontaneous resolution, chronic recurrence to rapid and fatal progression [131]. LCH most frequently affects the bone (80%), the skin (33%), and the pituitary gland (25%) [132]. CNS involvement is seen in 25–50% of cases of LCH [133]. Clinical

symptoms depend on the site of CNS involvement. Diabetes insipidus is the most common manifestation followed by growth hormone deficiency [134].

The imaging manifestations of CNS LCH can be categorized into four groups [135]. Cranio-facial osteolytic lesions having typical beveled margins with or without a soft tissue component is most prevalent. Hypothalamic-pituitary region is the most frequently involved intracranial structure correlating with anterior pituitary hormone deficiency and diabetes insipidus [136]. There is thickening of the pituitary stalk due to infiltration by LCH granulomas, which may progress to space occupying pituitary or hypothalamus mass. The loss of Anti Diuretic Hormone granules corresponds to the loss of T1 hyperintense posterior pituitary bright spot. Meningeal lesions occur in less than one third of children with LCH, often adjacent to soft tissue or osseous lesions with T1 intermediate and T2 hyperintensity signal intensity and homogeneous enhancement [135].

Circumventricular region which includes pineal gland, choroid plexus and ependyma and are located outside blood-brain-barrier. The concurrent involvement of pituitary and pineal gland can be due to functional interaction and direct infiltration by the disease process [137]. Leukoencephalopathy pattern involving the cerebellar white matter (most common), pons, and/or periventricular white matter can be seen as symmetric patchy T2 hyperintense and T1 hypointense lesions [135,136]. Cerebellar atrophy can also be seen (Figure 26) [138].



(A)



(B)

Figure 26. Cont.



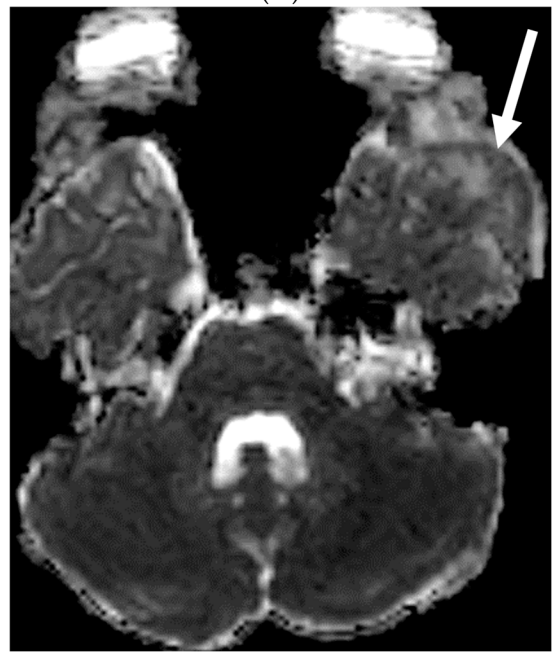
(C)



(D)



(E)



(F)

Figure 26. Cont.

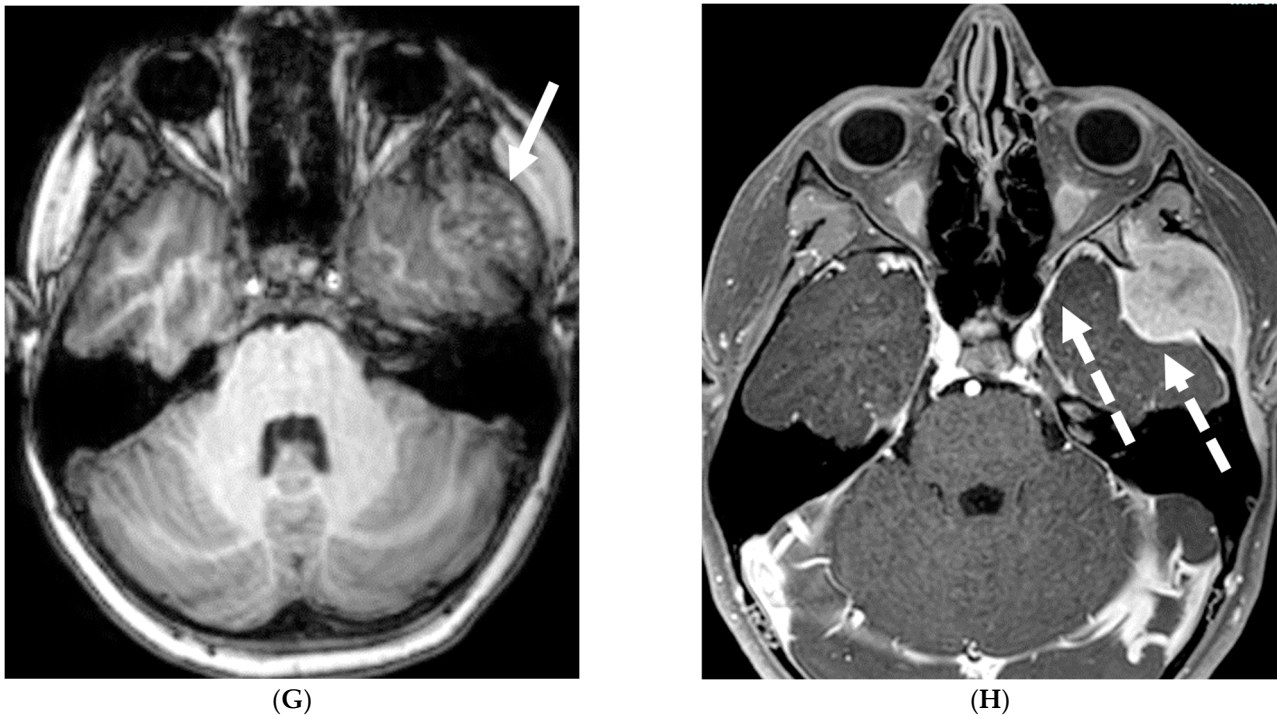


**Figure 26.** Axial CT bone (A) and brain (B) windows, Axial T2 (C), Axial FLAIR (D), Trace DWI (E), ADC (F), Axial T1 pre (G) and post contrast (H): 9-year-old boy with palpable left cheek mass. There is an ovoid destructive mass (white arrows) in the greater sphenoid wing bulging into the middle cranial fossa with heterogeneous slight restricted diffusivity. The lesion avidly enhances with dural thickening and enhancement (dashed arrows) extending toward Meckel cave and the cavernous sinus. Pathology: LCH.

## 6. Conclusions

Pediatric meningeal diseases exhibit overlapping imaging features that pose diagnostic challenges. An imaging-based classification, emphasizing parenchymal and associated findings, can aid in systemic evaluation. Integrating these radiological patterns with clinical and laboratory data helps improve diagnostic accuracy. This approach is crucial for guiding patient management, particularly in acute settings where imaging often precedes definitive diagnostic tests.

**Author Contributions:** Conceptualization, V.K. and D.D.P., Methodology, D.D.P. and S.L., software, D.D.P. and S.L., Resources, D.D.P., L.Z.F. and V.K., Writing—review and editing—D.D.P., L.Z.F. and S.L., Supervision—V.K. and L.Z.F., Project administration—V.K., Funding acquisition—V.K. All authors have read and agreed to the published version of the manuscript.

**Funding:** Publication made possible in part by support from the Nemours Grants for Open Access from Library Services and Department of Imaging, Nemours Children’s Health, Delaware.

**Conflicts of Interest:** The authors declare no conflicts of interest.

## References

1. Mohan, S.; Jain, K.K.; Arabi, M.; Shah, G.V. Imaging of Meningitis and Ventriculitis. *Neuroimaging Clin. N. Am.* **2012**, *22*, 557–583. [[CrossRef](#)]
2. Meltzer, C.C.; Fukui, M.B.; Kanal, E.; Smirniotopoulos, J.G. MR imaging of the meninges. Part I. Normal anatomic features and nonneoplastic disease. *Radiology* **1996**, *201*, 297–308. [[CrossRef](#)]
3. Bou, G.; Goldman-Yassen, A.; Morris, M.; Dutt, M.; Philbrook, P.; Gombolay, G. Differential Diagnosis of Leptomeningeal Enhancement in the Pediatric Population (P4-4.010). *Neurology* **2024**, *102* (Suppl. S1). [[CrossRef](#)]
4. Kastrup, O.; Wanke, I.; Maschke, M. Neuroimaging of infections of the central nervous system. *Semin Neurol.* **2008**, *28*, 511–522. [[CrossRef](#)] [[PubMed](#)]

5. Kralik, S.; Vallejo, J.; Kukreja, M.; Salman, R.; Orman, G.; Huisman, T.; Desai, N. Diagnostic Accuracy of MRI for Detection of Meningitis in Infants. *Am. J. Neuroradiol.* **2022**, *43*, 1350–1355. [[CrossRef](#)] [[PubMed](#)] [[PubMed Central](#)]
6. Lass-Flörl, C.; Mayr, A. Human Protothecosis. *Clin. Microbiol. Rev.* **2007**, *20*, 230–242. [[CrossRef](#)] [[PubMed](#)] [[PubMed Central](#)]
7. Thiele, D.; Bergmann, A. Protothecosis in human medicine. *Int. J. Hyg. Environ. Health* **2002**, *204*, 297–302. [[CrossRef](#)] [[PubMed](#)]
8. Lu, Y.; Zhang, X.; Ni, F.; Xia, W. Cutaneous Protothecosis with Meningitis Due to *Prototheca wickerhamii* in an Immunocompetent Teenager: Case Report and Literature Review. *Infect. Drug Resist.* **2021**, *14*, 2787–2794. [[CrossRef](#)]
9. Joerger, T.; Sulieman, S.; Carson, V.J.; Fox, M.D. Chronic Meningitis Due to *Prototheca zopfii* in an Adolescent Girl. *J. Pediatr. Infect. Dis. Soc.* **2021**, *10*, 370–372. [[CrossRef](#)] [[PubMed](#)] [[PubMed Central](#)]
10. Bathla, G.; Singh, A.; Policeni, B.; Agarwal, A.; Case, B. Imaging of neurosarcoidosis: Common, uncommon, and rare. *Clin. Radiol.* **2015**, *71*, 96–106. [[CrossRef](#)] [[PubMed](#)]
11. Bathla, G.; Watal, P.; Gupta, S.; Nagpal, P.; Mohan, S.; Moritani, T. Cerebrovascular Manifestations of Neurosarcoidosis: An Underrecognized Aspect of the Imaging Spectrum. *Am. J. Neuroradiol.* **2018**, *39*, 1194–1200. [[CrossRef](#)] [[PubMed](#)] [[PubMed Central](#)]
12. Fritz, D.; van de Beek, D.; Brouwer, M.C. Clinical features, treatment and outcome in neurosarcoidosis: Systematic review and meta-analysis. *BMC Neurol.* **2016**, *16*, 220. [[CrossRef](#)] [[PubMed](#)] [[PubMed Central](#)]
13. Jachiet, V.; Lhote, R.; Rufat, P.; Pha, M.; Haroche, J.; Crozier, S.; Dupel-Potier, C.; Psimaras, D.; Amoura, Z.; Aubart, F.C. Clinical, imaging, and histological presentations and outcomes of stroke related to sarcoidosis. *J. Neurol.* **2018**, *265*, 2333–2341. [[CrossRef](#)] [[PubMed](#)]
14. Herring, A.; Urich, H. Sarcoidosis of the central nervous system. *J. Neurol. Sci.* **1969**, *9*, 405–422. [[CrossRef](#)] [[PubMed](#)]
15. Conklin, J.; Silver, F.L.; Mikulis, D.J.; Mandell, D.M. Are acute infarcts the cause of leukoariosis? Brain mapping for 16 consecutive weeks. *Ann. Neurol.* **2014**, *76*, 899–904. [[CrossRef](#)] [[PubMed](#)]
16. Stern, B.J.; Royal, W.; Gelfand, J.M.; Clifford, D.B.; Tavee, J.; Pawate, S.; Berger, J.R.; Aksamit, A.J.; Krumholz, A.; Pardo, C.A.; et al. Definition and Consensus Diagnostic Criteria for Neurosarcoidosis: From the neurosarcoidosis consortium consensus group. *JAMA Neurol.* **2018**, *75*, 1546–1553. [[CrossRef](#)] [[PubMed](#)]
17. Hebel, R.; Dubaniewicz-Wybieralska, M.; Dubaniewicz, A. Overview of neurosarcoidosis: Recent advances. *J. Neurol.* **2015**, *262*, 258–267. [[CrossRef](#)] [[PubMed](#)] [[PubMed Central](#)]
18. Shah, R.; Roberson, G.; Curé, J. Correlation of MR Imaging Findings and Clinical Manifestations in Neurosarcoidosis. *Am. J. Neuroradiol.* **2009**, *30*, 953–961. [[CrossRef](#)] [[PubMed](#)] [[PubMed Central](#)]
19. Lexa, F.J.; Grossman, R.I. MR of sarcoidosis in the head and spine: Spectrum of manifestations and radiographic response to steroid therapy. *Am. J. Neuroradiol.* **1994**, *15*, 973–982. [[PubMed](#)] [[PubMed Central](#)]
20. Bagnato, F.; Stern, B.J. Neurosarcoidosis: Diagnosis, therapy and biomarkers. *Expert Rev. Neurother.* **2015**, *15*, 533–548. [[CrossRef](#)] [[PubMed](#)]
21. Christoforidis, G.A.; Spickler, E.M.; Recio, M.V.; Mehta, B.M. MR of CNS Sarcoidosis: Correlation of Imaging Features to Clinical Symptoms and Response to Treatment. *Am. J. Neuroradiol.* **1999**, *20*, 655–669. [[PubMed](#)] [[PubMed Central](#)]
22. Dumas, J.-L.; Valeyre, D.; Chapelon-Abric, C.; Belin, C.; Piette, J.-C.; Tandjaoui-Lambiotte, H.; Brauner, M.; Goldlust, D. Central Nervous System Sarcoidosis: Follow-Up at MR Imaging During Steroid Therapy. *Radiology* **2000**, *214*, 411–420. [[CrossRef](#)] [[PubMed](#)]
23. Bathla, G.; Freeman, C.; Moritani, T.; Song, J.; Srivastava, S.; Soni, N.; Derdeyn, C.; Mohan, S. Retrospective, dual-centre review of imaging findings in neurosarcoidosis at presentation: Prevalence and imaging sub-types. *Clin. Radiol.* **2020**, *75*, 796.e1–796.e9. [[CrossRef](#)] [[PubMed](#)]
24. Chiò, A.; Cocito, D.; Leone, M.; Giordana, M.; Mora, G.; Mutani, R.; Piemonte, T.; Valle d’Aosta Register for Guillain-Barré Syndrome. Guillain-Barré syndrome: A prospective, population-based incidence and outcome survey. *Neurology* **2003**, *60*, 1146–1150. [[CrossRef](#)] [[PubMed](#)]
25. Hughes, R.A.C.; Rees, J.H. Clinical and Epidemiologic Features of Guillain-Barré Syndrome. *J. Infect. Dis.* **1997**, *176* (Suppl. S2), S92–S98. [[CrossRef](#)] [[PubMed](#)]
26. Alter, M. The epidemiology of Guillain-Barré syndrome. *Ann. Neurol.* **1990**, *27* (Suppl. S7), S7–S12. [[CrossRef](#)] [[PubMed](#)]
27. Alkan, O.; Yildirim, T.; Tokmak, N.; Tan, M. Spinal MRI Findings of Guillain-Barré Syndrome. *J. Radiol. Case Rep.* **2009**, *3*, 25–28. [[CrossRef](#)] [[PubMed](#)] [[PubMed Central](#)]
28. Winer, J.B.; Hughes, R.A.; Anderson, M.J.; Jones, D.M.; Kangro, H.; Watkins, R.P. A prospective study of acute idiopathic neuropathy. II. Antecedent events. *J. Neurol. Neurosurg. Psychiatry* **1988**, *51*, 613–618. [[CrossRef](#)] [[PubMed](#)] [[PubMed Central](#)]
29. Dimachkie, M.M.; Barohn, R.J. Guillain-Barré syndrome and variants. *Neurol Clin.* **2013**, *31*, 491–510. [[CrossRef](#)] [[PubMed](#)] [[PubMed Central](#)]
30. van Doorn, P.A.; Ruts, L.; Jacobs, B.C. Clinical features, pathogenesis, and treatment of Guillain-Barré syndrome. *Lancet Neurol.* **2008**, *7*, 939–950. [[CrossRef](#)] [[PubMed](#)]
31. Fulbright, R.K.; Erdum, E.; Sze, G.; Byrne, T. Cranial nerve enhancement in the Guillain-Barré syndrome. *Am. J. Neuroradiol.* **1995**, *16* (Suppl. S4), 923–925. [[PubMed](#)] [[PubMed Central](#)]
32. Yikilmaz, A.; Doganay, S.; Gumus, H.; Per, H.; Kumandas, S.; Coskun, A. Magnetic resonance imaging of childhood Guillain-Barré syndrome. *Childs Nerv. Syst.* **2010**, *26*, 1103–1108. [[CrossRef](#)] [[PubMed](#)]

33. Byun, W.M.; Park, W.K.; Park, B.H.; Ahn, S.H.; Hwang, M.S.; Chang, J.C. Guillain-Barré syndrome: MR imaging findings of the spine in eight patients. *Radiology* **1998**, *208*, 137–141. [[CrossRef](#)] [[PubMed](#)]
34. Zuccoli, G.; Panigrahy, A.; Bailey, A.; Fitz, C. Redefining the Guillain-Barré Spectrum in Children: Neuroimaging Findings of Cranial Nerve Involvement. *Am. J. Neuroradiol.* **2011**, *32*, 639–642. [[CrossRef](#)] [[PubMed](#)] [[PubMed Central](#)]
35. Malhotra, A.; Zhang, M.; Wu, X.; Jindal, S.; Durand, D.; Makhani, N. MRI findings of optic pathway involvement in Miller Fisher syndrome in 3 pediatric patients and a review of the literature. *J. Clin. Neurosci.* **2017**, *39*, 63–67. [[CrossRef](#)] [[PubMed](#)]
36. Gallardo, E.; Sedano, M.J.; Orizaola, P.; Sánchez-Juan, P.; González-Suárez, A.; García, A.; Terán-Villagrà, N.; Ruiz-Soto, M.; Álvaro, R.L.; Berciano, M.T.; et al. Spinal nerve involvement in early Guillain-Barré syndrome: A clinico-electrophysiological, ultrasonographic and pathological study. *Clin. Neurophysiol.* **2015**, *126*, 810–819. [[CrossRef](#)] [[PubMed](#)]
37. Razali, S.N.O.; Arumugam, T.; Yuki, N.; Rozalli, F.I.; Goh, K.-J.; Shahrizaila, N. Serial peripheral nerve ultrasound in Guillain-Barré syndrome. *Clin. Neurophysiol.* **2016**, *127*, 1652–1656. [[CrossRef](#)] [[PubMed](#)]
38. Bosman, T.; Simonin, C.; Launay, D.; Caron, S.; Destée, A.; Defebvre, L. Idiopathic hypertrophic cranial pachymeningitis treated by oral methotrexate: A case report and review of literature. *Rheumatol. Int.* **2008**, *28*, 713–718. [[CrossRef](#)] [[PubMed](#)] [[PubMed Central](#)]
39. Takahashi, H.; Wada, A.; Yokoyama, Y.; Ishii, M.; Shibuya, K.; Suguro, T. Idiopathic Hypertrophic Spinal Pachymeningitis: A Case Report. *J. Orthop. Surg.* **2010**, *18*, 113–117. [[CrossRef](#)] [[PubMed](#)]
40. De Virgilio, A.; de Vincentiis, M.; Inghilleri, M.; Fabrini, G.; Conte, M.; Gallo, A.; Rizzo, M.I.; Greco, A. Idiopathic hypertrophic pachymeningitis: An autoimmune IgG4-related disease. *Immunol. Res.* **2017**, *65*, 386–394. [[CrossRef](#)] [[PubMed](#)]
41. Chan, S.-K.; Cheuk, W.; Chan, K.-T.; Chan, J.K.C. IgG4-related Sclerosing Pachymeningitis: A previously unrecognized form of central nervous system involvement in IgG4-related sclerosing disease. *Am. J. Surg. Pathol.* **2009**, *33*, 1249–1252. [[CrossRef](#)] [[PubMed](#)]
42. Shapiro, K.A.; Bové, R.M.; Volpicelli, E.R.; Mallery, R.M.; Stone, J.H. Relapsing course of Immunoglobulin G4-related pachymeningitis. *Neurology* **2012**, *79*, 604–606. [[CrossRef](#)] [[PubMed](#)]
43. Kupersmith, M.; Martin, V.; Heller, G.; Shah, A.; Mitnick, H. Idiopathic hypertrophic pachymeningitis. *Neurology* **2004**, *62*, 686–694. [[CrossRef](#)] [[PubMed](#)]
44. Karthik, S.; Bhanu, K.; Velayutham, S.; Jawahar, M. Hypertrophic pachymeningitis. *Ann. Indian Acad. Neurol.* **2011**, *14*, 203–204. [[CrossRef](#)] [[PubMed](#)]
45. Friedman, D.P.; Flanders, A.E. Enhanced MR imaging of hypertrophic pachymeningitis. *Am. J. Roentgenol.* **1997**, *169*, 1425–1428. [[CrossRef](#)] [[PubMed](#)]
46. Goyal, M.; Malik, A.; Mishra, N.K.; Gaikwad, S.B. Idiopathic hypertrophic pachymeningitis: Spectrum of the disease. *Neuroradiology* **1997**, *39*, 619–623. [[CrossRef](#)] [[PubMed](#)]
47. Menon, G.; Nair, S.; Sudhir, J.; Rao, B.R.M.; Mathew, A.; Bahuleyan, B. Childhood and adolescent meningiomas: A report of 38 cases and review of literature. *Acta Neurochir.* **2009**, *151*, 239–244. [[CrossRef](#)] [[PubMed](#)]
48. Greene, S.; Nair, N.; Ojemann, J.G.; Ellenbogen, R.G.; Avellino, A.M. Meningiomas in Children. *Pediatr. Neurosurg.* **2008**, *44*, 9–13. [[CrossRef](#)] [[PubMed](#)]
49. Pinto, P.S.; Huisman, T.A.; Ahn, E.; Jordan, L.C.; Burger, P.; Cohen, K.J.; Patay, Z.; Tekes, A. Magnetic resonance imaging features of meningiomas in children and young adults: A retrospective analysis. *J. Neuroradiol.* **2012**, *39*, 218–226. [[CrossRef](#)] [[PubMed](#)]
50. Rochat, P.; Johannesen, H.H.; Gjerris, F. Long-term follow up of children with meningiomas in Denmark: 1935 to 1984. *J. Neurosurg. Pediatr.* **2004**, *100* (Suppl. S2), 179–182. [[CrossRef](#)] [[PubMed](#)]
51. Tenenbaum, M. Extraparenchymal Lesions in Pediatric Patients. *Neuroimaging Clin. N. Am.* **2017**, *27*, 123–134. [[CrossRef](#)] [[PubMed](#)]
52. Louis, D.N.; Perry, A.; Reifenberger, G.; Von Deimling, A.; Figarella-Branger, D.; Cavenee, W.K.; Ohgaki, H.; Wiestler, O.D.; Kleihues, P.; Ellison, D.W. The 2016 World Health Organization Classification of Tumors of the Central Nervous System: A summary. *Acta Neuropathol.* **2016**, *131*, 803–820. [[CrossRef](#)] [[PubMed](#)]
53. Jiang, H.; Qiu, L.; Song, J.; Xu, D.; Sun, L.; Feng, Y.; Zhao, J.; Qian, J.; Yu, Z.; Peng, J. Clinical progression, pathological characteristics, and radiological findings in children with diffuse leptomeningeal glioneuronal tumors: A systematic review. *Front. Oncol.* **2022**, *12*, 970076. [[CrossRef](#)] [[PubMed](#)] [[PubMed Central](#)]
54. Ferracioli, S.F.; Tortora, M.; Godoy, L.F.d.S.; Casal, Y.R.; Lucato, L.T. Haberland Syndrome (*Encephalocraniocutaneous lipomatosis*) with Development of Diffuse Leptomeningeal Glioneuronal Tumor (DL-GNT) during Adolescence. *Clin. Neuroradiol.* **2024**, *34*, 973–976. [[CrossRef](#)]
55. Rodriguez, F.J.; Perry, A.; Rosenblum, M.K.; Krawitz, S.; Cohen, K.J.; Lin, D.; Mosier, S.; Lin, M.-T.; Eberhart, C.G.; Burger, P.C. Disseminated oligodendroglial-like leptomeningeal tumor of childhood: A distinctive clinicopathologic entity. *Acta Neuropathol.* **2012**, *124*, 627–641. [[CrossRef](#)] [[PubMed](#)]
56. Lakhani, D.; Mankad, K.; Chhabda, S.; Feizi, P.; Patel, R.; Sarma, A.; Pruthi, S. Diffuse Leptomeningeal Glioneuronal Tumor of Childhood. *Am. J. Neuroradiol.* **2020**, *41*, 2155–2159. [[CrossRef](#)] [[PubMed](#)] [[PubMed Central](#)]
57. Gardiman, M.P.; Fassan, M.; Orvieto, E.; D’avella, D.; Denaro, L.; Calderone, M.; Severino, M.; Scarsello, G.; Viscardi, E.; Perilongo, G. Diffuse Leptomeningeal Glioneuronal Tumors: A New Entity? *Brain Pathol.* **2010**, *20*, 361–366. [[CrossRef](#)] [[PubMed](#)] [[PubMed Central](#)]
58. Wolden, S.L.; Alektiar, K.M. Sarcomas Across the Age Spectrum. *Semin. Radiat. Oncol.* **2010**, *20*, 45–51. [[CrossRef](#)] [[PubMed](#)]

59. McCarville, M.B.; Spunt, S.L.; Pappo, A.S. Rhabdomyosarcoma in Pediatric atients: The good, the bad, and the unusual. *Am. J. Roentgenol.* **2001**, *176*, 1563–1569. [[CrossRef](#)] [[PubMed](#)]
60. Korinthenberg, R.; Edel, G.; Palm, D.; Müller, K.-M.; Brandt, M.; Müller, R.-P. Primary rhabdomyosarcoma of the leptomeninx: Clinical, neuroradiological and pathological aspects. *Clin. Neurol. Neurosurg.* **1984**, *86*, 301–305. [[CrossRef](#)] [[PubMed](#)]
61. Xu, F.; Casas, L.E.D.L.; Dobbs, J.L.J. Primary Meningeal Rhabdomyosarcoma in a Child With Hypomelanosis of Ito. *Arch. Pathol. Lab. Med.* **2000**, *124*, 762–765. [[CrossRef](#)] [[PubMed](#)]
62. Primary Meningeal Rhabdomyosarcoma-Rahul Nikam MD, Ashrith Kandula, Tushar Chandra, MD Affiliations: Nemours/Alfred I. duPont Hospital for Children, Wilmington, DE (Dr Nikam, Mr. Kandula); Nemours Children’s Hospital, Orlando, FL (Dr Chandra). Available online: [https://cdn.agilitycms.com/applied-radiology/PDFs/AR\\_09-21\\_Nikam\\_Guerbet.pdf](https://cdn.agilitycms.com/applied-radiology/PDFs/AR_09-21_Nikam_Guerbet.pdf) (accessed on 8 June 2024).
63. Palta, M.; Riedel, R.F.; Vredenburgh, J.J.; Cummings, T.J.; Green, S.; Chang, Z.; Kirkpatrick, J.P. Primary Meningeal Rhabdomyosarcoma. *Sarcoma* **2011**, *2011*, 312802. [[CrossRef](#)] [[PubMed](#)] [[PubMed Central](#)]
64. Peterson, E.E.; Riley, B.L.; Windsor, R.B. Pediatric Intracranial Hypotension and Post-Dural Puncture Headache. *Semin. Pediatr. Neurol.* **2021**, *40*, 100927. [[CrossRef](#)] [[PubMed](#)]
65. Schievink, W.I.; Maya, M.M.; Louy, C.; Moser, F.G.; Sloninsky, L. Spontaneous Intracranial Hypotension in Childhood and Adolescence. *J. Pediatr.* **2013**, *163*, 504–510.e3. [[CrossRef](#)] [[PubMed](#)]
66. Shah, L.M.; McLean, L.A.; Heilbrun, M.E.; Salzman, K.L. Intracranial Hypotension: Improved MRI Detection With Diagnostic Intracranial Angles. *Am. J. Roentgenol.* **2013**, *200*, 400–407. [[CrossRef](#)] [[PubMed](#)]
67. Yuh, E.L.; Dillon, W.P. Intracranial Hypotension and Intracranial Hypertension. *Neuroimaging Clin. N. Am.* **2010**, *20*, 597–617. [[CrossRef](#)] [[PubMed](#)]
68. Medina, J.H.; Abrams, K.; Falcone, S.; Bhatia, R.G. Spinal Imaging Findings in Spontaneous Intracranial Hypotension. *Am. J. Roentgenol.* **2010**, *195*, 459–464. [[CrossRef](#)] [[PubMed](#)]
69. Kemps, P.G.; Picarsic, J.; Durham, B.H.; Hélias-Rodzewicz, Z.; Hiemcke-Jiwa, L.; Bos, C.v.D.; van de Wetering, M.D.; van Noesel, C.J.M.; van Laar, J.A.M.; Verdijk, R.M.; et al. ALK-positive histiocytosis: A new clinicopathologic spectrum highlighting neurologic involvement and responses to ALK inhibition. *Blood* **2022**, *139*, 256–280. [[CrossRef](#)] [[PubMed](#)] [[PubMed Central](#)]
70. Aoki, Y.; Maeda, M.; Kishi, S.; Kogue, R.; Tanaka, F.; Umino, M.; Takeoka, M.; Hanaki, R.; Hirayama, J.; Yuasa, H.; et al. Central nervous system involvement of systemic ALK-positive histiocytosis with KIF5B-ALK fusion. *Radiol. Case Rep.* **2022**, *17*, 3867–3870. [[CrossRef](#)] [[PubMed](#)] [[PubMed Central](#)]
71. Wang, J.; Zheng, Y.; Xiong, Y. Imaging features of ALK-positive histiocytosis with neurological involvement: A case report and literature review. *Front. Oncol.* **2024**, *14*, 1333519. [[CrossRef](#)] [[PubMed](#)] [[PubMed Central](#)]
72. Liu, H.-J.; Wang, W.-Y.; Tang, Y.; Zhao, S.; Zhang, W.-Y.; Yan, J.-Q.; Liu, W.-P. Multisystem ALK-positive histiocytosis: A multi-case study and literature review. *Orphanet J. Rare Dis.* **2023**, *18*, 53. [[CrossRef](#)] [[PubMed](#)]
73. Vaswani, A.K.; Nizamani, W.M.; Ali, M.; Aneel, G.; Shahani, B.K.; Hussain, S. Diagnostic Accuracy of Contrast-Enhanced FLAIR Magnetic Resonance Imaging in Diagnosis of Meningitis Correlated with CSF Analysis. *ISRN Radiol.* **2014**, *2014*, 578986. [[CrossRef](#)] [[PubMed](#)] [[PubMed Central](#)]
74. Jaremko, J.L.; Moon, A.S.; Kumbala, S. Patterns of complications of neonatal and infant meningitis on MRI by organism: A 10 year review. *Eur. J. Radiol.* **2011**, *80*, 821–827. [[CrossRef](#)] [[PubMed](#)]
75. Chiang, S.S.; Khan, F.A.; Milstein, M.B.; Tolman, A.W.; Benedetti, A.; Starke, J.R.; Becerra, M.C. Treatment outcomes of childhood tuberculous meningitis: A systematic review and meta-analysis. *Lancet Infect. Dis.* **2014**, *14*, 947–957. [[CrossRef](#)]
76. Dian, S.; Hermawan, R.; van Laarhoven, A.; Immaculata, S.; Achmad, T.H.; Ruslami, R.; Anwar, F.; Soetikno, R.D.; Ganiem, A.R.; van Crevel, R. Brain MRI findings in relation to clinical characteristics and outcome of tuberculous meningitis. *PLoS ONE* **2020**, *15*, e0241974. [[CrossRef](#)] [[PubMed](#)] [[PubMed Central](#)]
77. Krishnan, N.; Renganathan, L. Tuberculous meningitis sequelae as basal cisternal calcifications. *J. Pediatr. Neurosci.* **2016**, *11*, 86–87. [[CrossRef](#)] [[PubMed](#)] [[PubMed Central](#)]
78. Khatri, G.D.; Krishnan, V.; Antil, N.; Saigal, G. Magnetic resonance imaging spectrum of intracranial tubercular lesions: One disease, many faces. *Pol. J. Radiol.* **2018**, *83*, e524–e535. [[CrossRef](#)] [[PubMed](#)] [[PubMed Central](#)]
79. Bomanji, J.B.; Gupta, N.; Gulati, P.; Das, C.J. Imaging in Tuberculosis. *Cold Spring Harb. Perspect. Med.* **2015**, *5*, a017814. [[CrossRef](#)] [[PubMed](#)] [[PubMed Central](#)]
80. Kralik, S.; O’Neill, D.; Kamer, A.; Rodriguez, E.; Ho, C. Radiological diagnosis of drop metastases from paediatric brain tumours using combination of 2D and 3D MRI sequences. *Clin. Radiol.* **2017**, *72*, 902.e13–902.e19. [[CrossRef](#)] [[PubMed](#)]
81. Silva, F.A.B.; Senerchia, A.A.; Cappellano, A.; Saba, N.; Chinelati, R.M.K.; Lederman, H. Medulloblastoma and Drop Metastasis: MRI Evaluation and Optimized Protocol. *Curr. Radiol. Rep.* **2015**, *3*, 26. [[CrossRef](#)]
82. Harrison, S.K.; Ditchfield, M.R.; Waters, K. Correlation of MRI and CSF cytology in the diagnosis of medulloblastoma spinal metastases. *Pediatr. Radiol.* **1998**, *28*, 571–574. [[CrossRef](#)] [[PubMed](#)]
83. Lisanti, C.; Carlin, C.; Banks, K.P.; Wang, D. Normal MRI Appearance and Motion-Related Phenomena of CSF. *Am. J. Roentgenol.* **2007**, *188*, 716–725. [[CrossRef](#)] [[PubMed](#)]
84. Singh, S.K.; Leeds, N.E.; Ginsberg, L.E. MR Imaging of Leptomeningeal Metastases: Comparison of Three Sequences. *Am. J. Roentgenol.* **2002**, *23*, 817–821. [[PubMed](#)] [[PubMed Central](#)]

85. Porto, L.; Kieslich, M.; Bartels, M.; Schwabe, D.; Zanella, F.E.; Du Mesnil, R. Leptomeningeal metastases in pediatrics: Magnetic resonance image manifestations and correlation with cerebral spinal fluid cytology. *Pediatr. Int.* **2010**, *52*, 541–546. [[CrossRef](#)] [[PubMed](#)]
86. Chamberlain, M.C. A Review of Leptomeningeal Metastases in Pediatrics. *J. Child Neurol.* **1995**, *10*, 191–199. [[CrossRef](#)] [[PubMed](#)]
87. Hatzoglou, V.; Karimi, S.; Diamond, E.L.; Lis, E.; Krol, G.; Holodny, A.I.; Young, R.J. Nonenhancing Leptomeningeal Metastases: Imaging Characteristics and Potential Causative Factors. *Neurohospitalist* **2016**, *6*, 24–28. [[CrossRef](#)]
88. Nguyen, A.; Nguyen, A.; Dada, O.T.; Desai, P.D.; Ricci, J.C.; Godbole, N.B.; Pierre, K.; Lucke-Wold, B. Leptomeningeal Metastasis: A Review of the Pathophysiology, Diagnostic Methodology, and Therapeutic Landscape. *Curr. Oncol.* **2023**, *30*, 5906–5931. [[CrossRef](#)] [[PubMed](#)] [[PubMed Central](#)]
89. Freilich, R.J.; Krol, G.; Deangelis, L.M. Neuroimaging and cerebrospinal fluid cytology in the diagnosis of leptomeningeal metastasis. *Ann. Neurol.* **1995**, *38*, 51–57. [[CrossRef](#)] [[PubMed](#)]
90. Liu, Z.-W.; Han, C.; Zhao, F.; Qiao, P.-G.; Wang, H.; Bao, X.-Y.; Zhang, Z.-S.; Yang, W.-Z.; Li, D.-S.; Duan, L. Collateral Circulation in Moyamoya Disease: A New Grading System. *Stroke* **2019**, *50*, 2708–2715. [[CrossRef](#)] [[PubMed](#)]
91. Tajmalzai, A.; Shirzai, A.; Najah, D.M. Early manifestation of Moyamoya syndrome in a 2-year-old child with Down syndrome. *Radiol. Case Rep.* **2021**, *16*, 1740–1744. [[CrossRef](#)] [[PubMed](#)] [[PubMed Central](#)]
92. Horie, N.; Morikawa, M.; Nozaki, A.; Hayashi, K.; Suyama, K.; Nagata, I. “Brush Sign” on Susceptibility-Weighted MR Imaging Indicates the Severity of Moyamoya Disease. *Am. J. Neuroradiol.* **2011**, *32*, 1697–1702. [[CrossRef](#)] [[PubMed](#)] [[PubMed Central](#)]
93. Ohta, T.; Tanaka, H.; Kuroiwa, T. Diffuse Leptomeningeal Enhancement, “Ivy Sign,” in Magnetic Resonance Images of Moyamoya Disease in Childhood: Case report. *Neurosurgery* **1995**, *37*, 1009–1012. [[CrossRef](#)] [[PubMed](#)]
94. Maeda, M.; Tsuchida, C. “Ivy Sign” on Fluid-Attenuated Inversion-Recovery Images in Childhood Moyamoya Disease. *Am. J. Neuroradiol.* **1999**, *20*, 1836–1838. [[PubMed](#)] [[PubMed Central](#)]
95. Liu, Z.; Han, C.; Wang, H.; Zhang, Q.; Li, S.; Bao, X.; Zhang, Z.; Duan, L. Clinical characteristics and leptomeningeal collateral status in pediatric and adult patients with ischemic moyamoya disease. *CNS Neurosci. Ther.* **2020**, *26*, 14–20. [[CrossRef](#)] [[PubMed](#)] [[PubMed Central](#)]
96. Komiyama, M.; Nakajima, H.; Nishikawa, M.; Yasui, T.; Kitano, S.; Sakamoto, H. Leptomeningeal contrast enhancement in moyamoya: Its potential role in postoperative assessment of circulation through the bypass. *Neuroradiology* **2001**, *43*, 17–23. [[CrossRef](#)] [[PubMed](#)]
97. Alonso, A.; Eisele, P.; Ebert, A.D.; Griebe, M.; Engelhardt, B.; Szabo, K.; Hennerici, M.G.; Gass, A. Leptomeningeal contrast enhancement and blood-CSF barrier dysfunction in aseptic meningitis. *Neurol. Neuroimmunol. Neuroinflamm.* **2015**, *2*, e164. [[CrossRef](#)] [[PubMed](#)] [[PubMed Central](#)]
98. Vossough, A.; Zimmerman, R.A.; Bilaniuk, L.T.; Schwartz, E.M. Imaging findings of neonatal herpes simplex virus type 2 encephalitis. *Neuroradiology* **2008**, *50*, 355–366. [[CrossRef](#)] [[PubMed](#)]
99. Mathur, M.; Johnson, C.E.; Sze, G. Fungal Infections of the Central Nervous System. *Neuroimaging Clin. N. Am.* **2012**, *22*, 609–632. [[CrossRef](#)] [[PubMed](#)]
100. McCarthy, M.W.; Kalasauskas, D.; Petraitis, V.; Petraitiene, R.; Walsh, T.J. Fungal Infections of the Central Nervous System in Children. *J. Pediatr. Infect. Dis. Soc.* **2017**, *6*, e123–e133. [[CrossRef](#)] [[PubMed](#)]
101. McCarthy, M.; Rosengart, A.; Schuetz, A.N.; Kontoyiannis, D.P.; Walsh, T.J. Mold infections of the central nervous system. *N. Engl. J. Med.* **2014**, *371*, 150–160. [[CrossRef](#)] [[PubMed](#)]
102. Gavito-Higuera, J.; Mullins, C.B.; Ramos-Duran, L.; Chacon, C.I.O.; Hakim, N.; Palacios, E. Fungal Infections of the Central Nervous System: A Pictorial Review. *J. Clin. Imaging Sci.* **2016**, *6*, 24. [[CrossRef](#)] [[PubMed](#)] [[PubMed Central](#)]
103. Aiken, A.H. Central Nervous System Infection. *Neuroimaging Clin. N. Am.* **2010**, *20*, 557–580. [[CrossRef](#)] [[PubMed](#)]
104. Gupta, R.K.; Jain, K.K.; Mittal, S.K.; Kumar, S. Imaging features of central nervous system fungal infections. *Neurol. India* **2007**, *55*, 241–250. [[CrossRef](#)] [[PubMed](#)]
105. Li, L.; Liu, W.; Cai, Q.; Liu, Y.; Hu, W.; Zuo, Z.; Ma, Q.; He, S.; Jin, K. Leptomeningeal enhancement of myelin oligodendrocyte glycoprotein antibody-associated encephalitis: Uncovering novel markers on contrast-enhanced fluid-attenuated inversion recovery images. *Front. Immunol.* **2023**, *14*, 1152235. [[CrossRef](#)] [[PubMed](#)] [[PubMed Central](#)]
106. Shahriari, M.; Sotirchos, E.S.; Newsome, S.D.; Yousem, D.M. MOGAD: How It Differs From and Resembles Other Neuroinflammatory Disorders. *Am. J. Roentgenol.* **2021**, *216*, 1031–1039. [[CrossRef](#)] [[PubMed](#)]
107. Gadde, J.A.; Wolf, D.S.; Keller, S.; Gombolay, G.Y. Rate of Leptomeningeal Enhancement in Pediatric Myelin Oligodendrocyte Glycoprotein Antibody-Associated Encephalomyelitis. *J. Child Neurol.* **2021**, *36*, 1042–1046. [[CrossRef](#)] [[PubMed](#)] [[PubMed Central](#)]
108. Valencia-Sanchez, C.; Guo, Y.; Krecke, K.N.; Chen, J.J.; Redenbaugh, V.; Montalvo, M.; Elsbernd, P.M.; Tillema, J.; Lopez-Chiriboga, S.; Budhram, A.; et al. Cerebral Cortical Encephalitis in Myelin Oligodendrocyte Glycoprotein Antibody-Associated Disease. *Ann. Neurol.* **2023**, *93*, 297–302. [[CrossRef](#)] [[PubMed](#)] [[PubMed Central](#)]
109. Potentas-Policewicz, M.; Fijolek, J. Granulomatosis with polyangiitis: Clinical characteristics and updates in diagnosis. *Front. Med.* **2024**, *11*, 1369233. [[CrossRef](#)] [[PubMed](#)] [[PubMed Central](#)]
110. Fragoulis, G.E.; Lionaki, S.; Venetsanopoulou, A.; Vlachoyiannopoulos, P.G.; Moutsopoulos, H.M.; Tzioufas, A.G. Central nervous system involvement in patients with granulomatosis with polyangiitis: A single-center retrospective study. *Clin. Rheumatol.* **2018**, *37*, 737–747. [[CrossRef](#)] [[PubMed](#)]

111. Zhang, W.; Zhou, G.; Shi, Q.; Zhang, X.; Zeng, X.-F.; Zhang, F.-C. Clinical analysis of nervous system involvement in ANCA-associated systemic vasculitides. *Clin. Exp. Rheumatol.* **2009**, *27* (Suppl. S52), S65–S69. [[PubMed](#)]
112. Zheng, Y.; Zhang, Y.; Cai, M.; Lai, N.; Chen, Z.; Ding, M. Central Nervous System Involvement in ANCA-Associated Vasculitis: What Neurologists Need to Know. *Front. Neurol.* **2019**, *9*, 1166. [[CrossRef](#)] [[PubMed](#)] [[PubMed Central](#)]
113. Murphy, J.M.; Gomez-Anson, B.; Gillard, J.H.; Antoun, N.M.; Cross, J.; Elliott, J.D.; Lockwood, M. Wegener Granulomatosis: MR Imaging Findings in Brain and Meninges. *Radiology* **1999**, *213*, 794–799. [[CrossRef](#)] [[PubMed](#)]
114. Guzman-Soto, M.I.; Kimura, Y.; Romero-Sanchez, G.; Cienfuegos-Alvear, J.A.; Candanedo-Gonzalez, F.; Kimura-Sandoval, Y.; Sanchez-Nava, D.A.; Alonso-Ramon, I.; Hinojosa-Azaola, A. From Head to Toe: Granulomatosis with Polyangiitis. *RadioGraphics* **2021**, *41*, 1973–1991. [[CrossRef](#)] [[PubMed](#)]
115. Eran, A.; Hodes, A.; Izbudak, I. Bilateral temporal lobe disease: Looking beyond herpes encephalitis. *Insights Imaging* **2016**, *7*, 265–274. [[CrossRef](#)] [[PubMed](#)] [[PubMed Central](#)]
116. Titulaer, M.J.; McCracken, L.; Gabilondo, I.; Armangue, T.; Glaser, C.; Iizuka, T.; Honig, L.S.; Benseler, S.M.; Kawachi, I.; Martinez-Hernandez, E.; et al. Treatment and prognostic factors for long-term outcome in patients with anti-NMDA receptor encephalitis: An observational cohort study. *Lancet Neurol.* **2013**, *12*, 157–165. [[CrossRef](#)] [[PubMed](#)] [[PubMed Central](#)]
117. Zhang, L.; Wu, M.-Q.; Hao, Z.-L.; Chiang, S.M.V.; Shuang, K.; Lin, M.-T.; Chi, X.-S.; Fang, J.-J.; Zhou, D.; Li, J.-M. Clinical characteristics, treatments, and outcomes of patients with anti-N-methyl-D-aspartate receptor encephalitis: A systematic review of reported cases. *Epilepsy Behav.* **2017**, *68*, 57–65. [[CrossRef](#)] [[PubMed](#)]
118. Gabilondo, I.; Saiz, A.; Galán, L.; González, V.; Jadraque, R.; Sabater, L.; Sans, A.; Sempere, A.; Vela, A.; Villalobos, F.; et al. Analysis of relapses in anti-NMDAR encephalitis. *Neurology* **2011**, *77*, 996–999. [[CrossRef](#)] [[PubMed](#)]
119. Irani, S.R.; Bera, K.; Waters, P.; Zuliani, L.; Maxwell, S.; Zandi, M.S.; Friese, M.A.; Galea, I.; Kullmann, D.M.; Beeson, D.; et al. N-methyl-D-aspartate antibody encephalitis: Temporal progression of clinical and paraclinical observations in a predominantly non-paraneoplastic disorder of both sexes. *Brain* **2010**, *133 Pt 6*, 1655–1667. [[CrossRef](#)] [[PubMed](#)] [[PubMed Central](#)]
120. Kelley, B.; Patel, S.; Marin, H.; Corrigan, J.; Mitsias, P.; Griffith, B. Autoimmune Encephalitis: Pathophysiology and Imaging Review of an Overlooked Diagnosis. *Am. J. Neuroradiol.* **2017**, *38*, 1070–1078. [[CrossRef](#)] [[PubMed](#)] [[PubMed Central](#)]
121. Park, J.K.; Lee, E.J.; Kim, K.K. Isolated Leptomeningeal Enhancement in Anti-N-Methyl D-Aspartate Receptor Encephalitis: The Diagnostic Value of Contrast-Enhanced Fluid-Attenuated Inversion Recovery Imaging. *J. Korean Soc. Radiol.* **2022**, *83*, 945–950. [[CrossRef](#)] [[PubMed](#)] [[PubMed Central](#)]
122. Agarwal, A.; Kapur, G.; Altinok, D. Childhood posterior reversible encephalopathy syndrome: Magnetic resonance imaging findings with emphasis on increased leptomeningeal FLAIR signal. *Neuroradiol. J.* **2015**, *28*, 638–643. [[CrossRef](#)] [[PubMed](#)] [[PubMed Central](#)]
123. Ishikura, K.; Ikeda, M.; Hamasaki, Y.; Hataya, H.; Shishido, S.; Asanuma, H.; Nishimura, G.; Hiramoto, R.; Honda, M. Posterior Reversible Encephalopathy Syndrome in Children: Its High Prevalence and More Extensive Imaging Findings. *Am. J. Kidney Dis.* **2006**, *48*, 231–238. [[CrossRef](#)] [[PubMed](#)]
124. Bartynski, W.S. Posterior Reversible Encephalopathy Syndrome, Part 1: Fundamental Imaging and Clinical Features. *Am. J. Neuroradiol.* **2008**, *29*, 1036–1042. [[CrossRef](#)] [[PubMed](#)] [[PubMed Central](#)]
125. Hamilton, B.E.; Nesbit, G.M. Delayed CSF Enhancement in Posterior Reversible Encephalopathy Syndrome. *Am. J. Neuroradiol.* **2008**, *29*, 456–457. [[CrossRef](#)] [[PubMed](#)] [[PubMed Central](#)]
126. Aylett, S. Sturge-Weber syndrome. *Ann. Indian Acad. Neurol.* **2007**, *10* (Suppl. S1), S55–S58. [[CrossRef](#)]
127. Bar, C.; Pedespan, J.; Boccara, O.; Garcelon, N.; Levy, R.; Grévent, D.; Boddaert, N.; Nabbout, R. Early magnetic resonance imaging to detect presymptomatic leptomeningeal angioma in children with suspected Sturge–Weber syndrome. *Dev. Med. Child Neurol.* **2020**, *62*, 227–233. [[CrossRef](#)] [[PubMed](#)]
128. Adams, M.; Aylett, S.; Squier, W.; Chong, W. A Spectrum of Unusual Neuroimaging Findings in Patients with Suspected Sturge-Weber Syndrome. *Am. J. Neuroradiol.* **2009**, *30*, 276–281. [[CrossRef](#)] [[PubMed](#)] [[PubMed Central](#)]
129. Jezierska, M.; Stefanowicz, J.; Romanowicz, G.; Kosiak, W.; Lange, M. Langerhans cell histiocytosis in children—A disease with many faces. Recent advances in pathogenesis, diagnostic examinations and treatment. *Postepy. Dermatol. Alergol.* **2018**, *35*, 6–17. [[CrossRef](#)] [[PubMed](#)] [[PubMed Central](#)]
130. Ribeiro, B.N.d.F.; Muniz, B.C.; Marchiori, E. Langerhans cell histiocytosis with isolated meningeal involvement: Findings on magnetic resonance imaging. *Radiol. Bras.* **2018**, *51*, 343–344. [[CrossRef](#)] [[PubMed](#)] [[PubMed Central](#)]
131. Pyun, J.-M.; Park, H.; Moon, K.C.; Jeon, B. Late-Onset Langerhans Cell Histiocytosis with Cerebellar Ataxia as an Initial Symptom. *Case Rep. Neurol.* **2016**, *8*, 218–223. [[CrossRef](#)] [[PubMed](#)] [[PubMed Central](#)]
132. Haroche, J.; Cohen-Aubart, F.; Rollins, B.J.; Donadieu, J.; Charlotte, F.; Idbaih, A.; Vaglio, A.; Abdel-Wahab, O.; Emile, J.-F.; Amoura, Z. Histiocytoses: Emerging neoplasia behind inflammation. *Lancet Oncol.* **2017**, *18*, e113–e125. [[CrossRef](#)] [[PubMed](#)]
133. Grois, N.; Fahrner, B.; Arceci, R.J.; Henter, J.-I.; McClain, K.; Lassmann, H.; Nanduri, V.; Prosch, H.; Prayer, D.; Histiocyte Society CNS LCH Study Group. Central Nervous System Disease in Langerhans Cell Histiocytosis. *J. Pediatr.* **2010**, *156*, 873–881.e1. [[CrossRef](#)] [[PubMed](#)]
134. Grois, N.; Pötschger, U.; Prosch, H.; Minkov, M.; Arico, M.; Braier, J.; Henter, J.; Janka-Schaub, G.; Ladisch, S.; Ritter, J.; et al. Risk factors for diabetes insipidus in langerhans cell histiocytosis. *Pediatr. Blood Cancer* **2006**, *46*, 228–233. [[CrossRef](#)] [[PubMed](#)]
135. Gabbay, L.B.; Leite, C.d.C.; Andriola, R.S.; Pinho, P.d.C.; Lucato, L.T. Histiocytosis: A review focusing on neuroimaging findings. *Arq. Neuro-Psiquiatr.* **2014**, *72*, 548–558. [[CrossRef](#)] [[PubMed](#)]

136. Prayer, D.; Grois, N.; Prosch, H.; Gadner, H.; Barkovich, A.J. MR Imaging Presentation of Intracranial Disease Associated with Langerhans Cell Histiocytosis. *Am. J. Neuroradiol.* **2004**, *25*, 880–891. [[PubMed](#)] [[PubMed Central](#)]
137. Grois, N.; Prosch, H.; Waldhauser, F.; Minkov, M.; Strasser, G.; Steiner, M.; Unger, E.; Prayer, D. Pineal gland abnormalities in Langerhans cell histiocytosis. *Pediatr. Blood Cancer* **2004**, *43*, 261–266. [[CrossRef](#)] [[PubMed](#)]
138. Martin-Duverneuil, N.; Idbaih, A.; Hoang-Xuan, K.; Donadieu, J.; Genereau, T.; Guillevin, R.; Chiras, J.; French Langerhans Cell Histiocytosis Study Group. MRI features of neurodegenerative Langerhans cell histiocytosis. *Eur. Radiol.* **2006**, *16*, 2074–2082. [[CrossRef](#)] [[PubMed](#)]

**Disclaimer/Publisher’s Note:** The statements, opinions and data contained in all publications are solely those of the individual author(s) and contributor(s) and not of MDPI and/or the editor(s). MDPI and/or the editor(s) disclaim responsibility for any injury to people or property resulting from any ideas, methods, instructions or products referred to in the content.